

RIGA TECHNICAL UNIVERSITY

Faculty of Power and Electrical Engineering
Institute of Industrial Electronics and Electrical Engineering

Kaspars Kroics

Doctoral Student of the Study Programme “Computerized Control of Electrical Technologies”

**DEVELOPMENT OF SUPERCAPACITOR
BASED DEVICES FOR ELECTRIC DRIVE
RETROFIT**

Summary of the Doctoral Thesis

Scientific supervisors

Dr. sc. ing. **LEONARDS LATKOVSKIS**

Dr. sc. ing. VIESTURS BRAZIS

RTU Press
Riga 2018

Kroics, K. Development of Supercapacitor Based Devices for Electric Drive Retrofit. Summary of the Doctoral Thesis. Riga: RTU Press, 2018. 52 p.

Published in accordance with the Resolution of the IEE Institute, dated on 27th August 2018, Minutes No. 127.

ISBN 978-9934-22-190-3 (print)
978-9934-22-191-0 (pdf)

DOCTORAL THESIS PROPOSED TO RIGA TECHNICAL UNIVERSITY FOR THE PROMOTION TO THE SCIENTIFIC DEGREE OF DOCTOR OF ENGINEERING SCIENCES

To be granted the scientific degree of Doctor of Engineering Sciences, the present Doctoral Thesis has been submitted for the defence at the open meeting of RTU Promotion Council on 7 December 2018 at the Faculty of Power and Electrical Engineering of Riga Technical University, 12/1 Azenes Street, Room 212.

OFFICIAL REVIEWERS

Professor Dr. sc. ing. Oskars Krievs
Riga Technical University

Dr. sc. ing. Mariusz Zdanowski
Warsaw University of Technology, Poland

Dr. sc. ing. Dimitar Arnaudov
The Technical University of Sofia, Bulgaria

DECLARATION OF ACADEMIC INTEGRITY

I hereby declare that the Doctoral Thesis submitted for the review to Riga Technical University for the promotion to the scientific degree of Doctor of Engineering Sciences is my own. I confirm that the Doctoral Thesis had not been submitted to any other university for the promotion to a scientific degree.

Kaspars Kroics (signature)

Date:

The Doctoral Thesis has been written in Latvian. It consists of Introduction; 5 chapters; Conclusions; 137 figures; 3 tables; the total number of pages is 143. The Bibliography contains 184 titles.

Content

General Description of the Doctoral Thesis.....	5
Topicality.....	5
Goal and objectives of the Research	5
Research Methods and Tools	5
Scientific novelties	6
Practical Significance of the Research	6
Thesis Statements to Be Defended.....	6
Dissemination of Results.....	7
Publications	8
Introduction.....	10
1. Utilization of energy storage into electrical drive systems	11
2. Development of regenerative braking test bench to investigate energy recovery in electric transport	12
2.1. Development of regenerative braking test bench.....	12
2.2. Development of supercapacitor based modernization device for lead-acid powered light electric vehicle retrofit.....	14
3. Current ripple reduction by utilization of coupled inductors in high power density power electronics converters.....	20
3.1. Inversely coupled inductor for two phase interleaved DC-DC converter.....	20
3.2. Current ripple reducing by using coupled inductor in multiphase interleaved converters.....	23
3.3. Application of directly and inversely coupled inductor combination in DC-DC	25
4. Modernization device for ICE starting improvement	28
4.1. The starting process of the ICE	28
4.2. Supercapacitor based modernization device for ICE starting improvement.....	29
4.3. Modernization device for ICE starting with active control.....	30
5. Development of modernization devices including DC-DC converters for frequency converter controlled electric drive retrofit to increase energy efficiency	33
5.1. Multiphase bi-directional DC-DC converter for energy storage integration	33
5.1.1. Topology selection	33
5.1.2. The control algorithm.....	35
5.1.3. The hardware.....	38
5.1.4. The test bench and experimental results	39
5.2. The ISOP forward converter and proposed voltage balancing method for low voltage supercapacitor module integration	42
5.2.1. Converter description	42
5.2.2. The proposed balancing method	43
5.2.3. The prototype and test results	45
Conclusions.....	46
Literature.....	48

General Description of the Doctoral Thesis

Topicality

The role of electric drive in everyday life is crucial, as today more than 70 % [1] of the world's electricity consumption is used in one of the types of electric drive. Electric drive is used not only in transport or industry, but also in the household and many other applications. Inefficient solutions are still used in many types of electric drives, for example, only about 5 % [2] of all installed elevators use solutions that utilize braking energy efficiently.

The transport sector is responsible for 30 % of all energy consumption in the European Union [3], which causes not only CO₂ but also other harmful emissions into the environment. As more and more electricity is produced from renewable energy sources, mainly through solar and wind power, the substitution of vehicles equipped with internal combustion engines is encouraged through various subsidies and by investing public funds in the development of electric, auto-related technologies, which partially or fully utilizes electrical power. It is projected that before 2020 the output of electric cars will reach 100,000 units per year [4]. For a long time, trolleybuses, trams, electric trains, special-purpose, and slow-moving electric vehicles have been widely used in transport. They are powered by either lithium-ion or lead-acid batteries. Their performance and efficiency can be enhanced by using a supercapacitor based modernization device that would increase battery life, more efficient use of braking energy storage, and efficiency at peak power. As the price of supercapacitors tends to decrease, it is essential to continue research on the use of such devices in small power vehicles as well as in other applications.

Goal and objectives of the research

The aim of the work is to develop perspective electric drive modernization equipment with super-capacitor electric energy storages and to study, improve and develop power electronics converters intended for them. To achieve the goal, the following tasks are set:

- to develop a test bench for studying recovery systems of regenerative braking energy in electric drive;
- to investigate the application of magnetically coupled elements in DC-DC converters;
- to develop a control algorithm for multi-phase DC-DC converter topology that works in the boundary conduction mode;
- to study the possibility of improving the internal combustion engine starting system by using supercapacitors;
- to develop supercapacitor based modernization kit that improves the efficiency of light electric vehicles;
- to develop bi-directional DC-DC converter for supercapacitor based modernization device for use in electric variable speed drives systems equipped with a frequency converter.

Research methods and tools

- Matlab/Simulink was used to develop detailed models for studying the control systems of electric transport and modernization devices.
- PSIM computer program was used to study power electronics converter topologies and control methods.

- MS Excel program was used to obtain graphs using the acquired analytical expressions.
- IAR Embedded Workbench was used to develop software code for microcontroller, Altium Designer – to design PCB, FEMM – for magnetic field simulation.
- Different types of multimeters and oscilloscopes were used to obtain experimental results in case of power electronics converter testing.
- To provide experiments with hardware, the technical base and equipment of the Riga Technical University – power supplies, power analyzers, signal generators, and other equipment was used.

Scientific novelty

- A new multi-level converter voltage balancing method has been developed.
- A new control method for the DC-DC converter operation in boundary conduction mode to reduce the size of the magnetics components was developed.
- An algorithm for selection of analog data measurement times to reduce the effect of electromagnetic interference on measurements was developed.
- A solution for the improvement of internal combustion engine startup processes using supercapacitors and a controllable switch was found.
- A supercapacitor based modernization kit with an independent control system and new control algorithms for improving the performance and energy efficiency of battery-powered light electric vehicles was developed.
- Analytical description of current ripples in DC-DC converters with coupled inductors was developed for improved construction of coupled inductors.

Practical significance of the research

- Supercapacitor based modernization conversion kit can be used in practical applications, increasing vehicle power and efficiency.
- The acquired mathematical expressions describing current ripple in magnetically coupled inductors can be used in practical engineering calculations.
- Modernization kit with supercapacitors connected to the 3-phase frequency converter DC bus can be used to increase the energy efficiency of electric drive and provide continuous power to the drive system.
- The proposed balancing method can be used in cases where it is not possible to implement a sophisticated algorithm that controls the voltage by using digital control.
- The control method for a converter operating in boundary conduction mode can be used in practical applications, increasing the power density of the converter.

Thesis statements to be defended

1. The modernization device with supercapacitors, which is proposed to retrofit electric vehicle equipped with lead acid batteries, allows to extend the battery life and increase the overall energy efficiency of the traction drive system. The size of the power electronics converters for the vehicle should be as small as possible. It is possible to develop easy to produce magnetically coupled inductor that allows reducing the current ripple of a four-phase DC-DC converter by an average of 20 %, increase the efficiency of the converter and reduce its size.

2. Utilization of supercapacitors in combination with power electronics solutions for starting an internal combustion engine allows extending the lifetime of lead-acid batteries, reduce the required volume and price of supercapacitors, reduce the voltage drop at start-up phase and the peak current through the starter motor, and allow to successfully start engine in the case of a discharged battery.
3. The application of supercapacitors has a perspective of accumulating recuperative braking energy of elevators, the use of specially adapted DC-DC converters allows optimal utilization of the capacity of energy storage and the achieving additional energy efficiency and reduction of the peak power consumed by elevator drive system. In this application, the dynamic response of the converter to the transient processes is important. The multiphase converter topology and operation in critical current or discontinuous current mode enables the creation of a converter with short response time and small size. By using the novel control algorithm, it is possible to create a multi-phase converter with low input and output power pulses without a current sensor and a control loop in each of the phases.
4. Since the supercapacitor voltage is low, many applications require the use of an isolated DC-DC converter. Using multi-level topology allows the use of cheaper transistors with better parameters and increases the efficiency of the converter, but balancing the voltages of the capacitive voltage divider should be addressed. Voltage balancing can be achieved without a special sophisticated control system by introducing new schematic solutions that can operate independently from the converter control system.

Dissemination of results

The main results of this Thesis have been presented in the following international scientific conferences:

- 14th International Scientific Conference “Engineering for Rural Development”, Jelgava, Latvia, 20–22 May 2015.
- 15th International Scientific Conference on Engineering for Rural Development, Latvia, Jelgava, 2016, 23–24 May 2016.
- 57th International Scientific Conference on Power and Electrical Engineering of Riga Technical University (RTUCON), 13–14 Oct. 2016.
- IEEE International Power Electronics and Motion Control Conference (PEMC), 25–28 Sept. 2016.
- 18th European Conference on Power Electronics and Applications (EPE’16 ECCE Europe), 5–9 Sept. 2016.
- PCIM Europe 2016; International Exhibition and Conference for Power Electronics, Intelligent Motion, Renewable Energy and Energy Management, 10–12 May 2016.
- 56th International Scientific Conference on Power and Electrical Engineering of Riga Technical University (RTUCON), 14 Oct. 2015.
- 9th International Conference on Compatibility and Power Electronics (CPE), 24–26 June 2015.
- Proceedings of PCIM Europe 2015; International Exhibition and Conference for Power Electronics, Intelligent Motion, Renewable Energy and Energy Management, 19–20 May 2015.

Publications

- Kroics, K., Zakis, J. “Multiphase Interleaved DC-DC Converter with Directly and Inversely Coupled Inductors,” in 57th International Scientific Conference on Power and Electrical Engineering of Riga Technical University (RTU CON 2016): Proceedings, Latvia, Riga, 13–14 October 2016 (SCOPUS).
- Kroics, K., Zakis, J., Suzdalenko, A., Gaigals, G. “A Simplified Approach to Input Voltage Balancing for Series Connected Isolated DC-DC Converters”, in 2016 18th European Conference on Power Electronics and Applications (EPE’16 ECCE Europe): Proceedings, Germany, Karlsruhe, 5–9 September 2016 (SCOPUS).
- Kroics, K., Sokolovs, A. “Interleaved DC-DC Converter with Discrete Duty Cycle and Open Loop Control,” Latvian Journal of Physics and Technical Sciences, 2016, Vol. 53, No. 4, pp.14–21 (SCOPUS).
- K. Kroics, A. Sokolovs, L. Grigans, U. Sirmelis. “ISOP converter with simplified voltage balance control,” in Proceedings of “International Exhibition and Conference for Power Electronics, Intelligent Motion, Renewable Energy and Energy Management” (PCIM Europe 2016), Germany, Nuremberg, 2016, pp. 1–8 (SCOPUS).
- Kroics, K., Bražis, V. Supercapacitor Based Storage System for Efficiency Improvement of Lead-Acid Powered Light Electric Vehicle, in Proceedings of 2016 IEEE International Power Electronics and Motion Control Conference (PEMC), Bulgaria, Varna, 25–30 September, 2016 (SCOPUS).
- K. Kroics, V. Bražis, “Ultracapacitor based storage system for lead-acid powered light electric vehicle retrofit,” in Proceedings of 15th International Scientific Conference on Engineering for Rural Development, Latvia, Jelgava, 2016, pp. 1386–1394 (SCOPUS).
- Kroics, K. “Bi-directional two level 6-phase DC-DC converter for energy storage application,” in Proceedings of “International Exhibition and Conference for Power Electronics, Intelligent Motion, Renewable Energy and Energy Management” (PCIM Europe 2015), Germany, Nuremberg, 2015, pp. 1–8 (SCOPUS).
- K. Kroics “Simulation Based Analysis of Digitally Controlled 4-phase DC-DC Converter with Coupled Inductors,” in Proceedings of 9th International Conference “Environment. Technology. Resources”, Latvia, Rezekne, 2015, pp. 89–95 (SCOPUS).
- K. Kroics, V. Brazis, U. Sirmelis “Voltage Balance Control of Two-Level DC-DC Converter,” in Proceedings of 14th International Scientific Conference “Engineering for Rural Development”, Latvia, Jelgava, 2015, pp. 402–407 (SCOPUS).
- K. Kroics, U. Sirmelis, L. Grigans, V. Brazis “Digitally Controlled 4-Phase Interleaved DC-DC Converter with Coupled Inductors for Storage Application in Microgrid,” in Proceedings of 9th International Conference on Compatibility and Power Electronics (CPE 2015), Portugal, Costa da Caparica, 2015, pp. 504–509 (SCOPUS).
- K. Kroics “System for Start of Internal Combustion Engine with Hybrid Battery-Supercapacitor Source,” in Proceedings of 56th International Scientific Conference on Power and Electrical Engineering of Riga Technical University (RTU CON 2015), Latvia, Riga, 2015, pp. 259–263 (SCOPUS).

- K. Kroics, U. Sirmelis, L. Grigans “Digitally Controlled 4-Phase Bi-Directional Interleaved Dc-Dc Converter with Coupled Inductors,” in *Latvian Journal of Physics and Technical Sciences*, Vol. 52, No. 4, 2015, pp. 18–31 (SCOPUS).
- K. Kroics, V. Brazis “Digitally Controlled Synchronous Buck-Boost Converter for Ultracapacitor Based Energy Storage Application,” in *Proceedings of 13th International Scientific Conference “Engineering for Rural Development”*, Vol. 13, Latvia, Jelgava, 2014, pp. 385–390 (SCOPUS).
- K. Kroics “Ostas konteineru krānu efektivitātes uzlabošana ar superkondensatoru enerģijas uzkrājējiem,” in *Proceedings of International Student Conference “Human. Environment. Technology”*, 2014, pp. 88–96.
- V. Brazis, K. Kroics, L. Grigans “Scientific Laboratory Platform for Testing the Electric Vehicle Equipped with DC Drive,” *Latvian Journal of Physics and Technical Sciences*, 2014, Vol. 51, No. 5, pp. 56–64 (SCOPUS).
- K. Kroics, U. Sirmelis, V. Brazis “Design of Coupled Inductor for Interleaved Boost Converter,” *Przegląd Elektrotechniczny*, 2014, No. 12, pp. 91–94 (SCOPUS).
- K. Kroics, U. Sirmelis, J. Cernovs “DSP Based Bi-Directional Interleaved DC-DC Converter for Energy Storage Application,” in *Proceedings of 12th International Scientific Conference “Engineering for Rural Development”*, Vol. 12, Latvia, Jelgava, 2013, pp. 441–445 (SCOPUS).
- K. Kroics “Standby Power Reduction of Auxiliary Power Supply for Digitally Controlled SMPS,” in *Proceedings of the 2nd Electronic International Interdisciplinary Conference (EIIC 2013)*, Slovakia, Zilina, 2013, pp. 396–401.
- K. Kroics “Digital Control of Variable Frequency Interleaved DC-DC Converter,” in *Proceedings of the 9th International Scientific and Practical Conference: “Environment. Technology. Resources.”*, Latvia, Rezekne, 2013, pp.124–129 (SCOPUS).
- K. Kroics, V. Brazis “A Digitally Controlled Test Bench for DC Electrical Drives,” in *Proceedings in Multidisciplinary Conference QUAESTI*, Slovakia, Zilina, 2013, pp. 166–170.

Introduction

Supercapacitor based modernization device integration into the electric drive system helps not only to store braking energy in drive systems where it is possible, but also to address other important issues, such as providing power supply to a drive system, in case of a primary power supply failure or during short voltage sags. Unplanned power supply interruptions in some applications can cause financial losses for the owner in excess of even a million dollars [5], it is also possible to reduce current harmonics, stabilize the voltage of the DC bus, and reduce the value of the current peak. As the electric drive life can reach several decades [6], there is still a large number of drive systems that are satisfactorily performing their intended task but are either energy non-efficient, or the state of health of energy storage used to supply power to drive system is bad. Replacing such drive systems with new ones requires large capital investments that pays off over a long period, and this period may be longer than the lifetime of the mechanical parts. Another approach is to partially modernize a running electric drive by replacing some parts with a new one or by adding a system with a modernization device. In this work the electric drive modernization device with supercapacitors was studied and developed, which allows to improve not only the power system efficiency of the drive system, but also prolong battery life, increase the peak power of the drive system, and ensure continuous power supply in case of power supply disconnection.

In order to provide an electric drive equipped with a modernization device, higher flexibility and efficiency of use, the supercapacitors cannot be connected directly to the DC bus, but a power electronics converter is required to control power flow. With the help of the bi-directional DC-DC converter, it is possible to provide different control algorithms depending on the particular application – the voltage of the DC bus, level of discharge/charge of the energy storage, reduction of peak power, and many other parameters can be regulated. Over the past 30 years, thousands of studies have been conducted on the optimization and improvement of the power electronics converters, but constantly more and more new topologies and improvements are still being published. In order to build a converter with the highest power density, efficiency, and affordability there is a need for collaboration between industry and research institutions, as well as large investments in human and financial resources. However, there is often a need for a converter that has high performance for some specific function, but the fact that some of the parameters are slightly lagging behind is not so important.

In this work, the possibilities of improving the converter were studied using the latest scientific solutions – integrated magnetic elements, multiphase topologies, multilevel topologies, and operation into boundary conduction mode. Prototypes of DC-DC converters, development and possible further small series production of which do not require specific passive components, high degree of integration, specific application integrated circuits, and other major investments, were developed during the scientific research. Besides converter control algorithms, specially adapted for supercapacitor based modernization equipment, were developed.

1. Utilization of energy storage in electrical drive systems

Induction motor or permanent magnet motor together with frequency converter is used more frequently to drive mechanisms where regenerative braking is possible. If the motor is pushed rotating faster than the synchronous speed, then it will move to regenerative braking mode and generate electricity. The main applications where braking energy is significant are electric transport and lifting devices. In a port crane application when a container is lowered, braking resistor creates a braking torque, and this will limit the hoisting speed. Motor output power dissipated in the braking resistor during braking process is used to heat the atmosphere. This energy can be stored and used for the next lifting cycle or supplied back to the grid, increasing the efficiency of the crane in such a way. The solution that will be analyzed and developed in this work is the use of supercapacitors in combination with bi-directional DC-DC converter to control energy flow (Fig. 1.1). The supercapacitor modernization device can be easily connected and used also to reduce peak power and supply power during voltage outages.

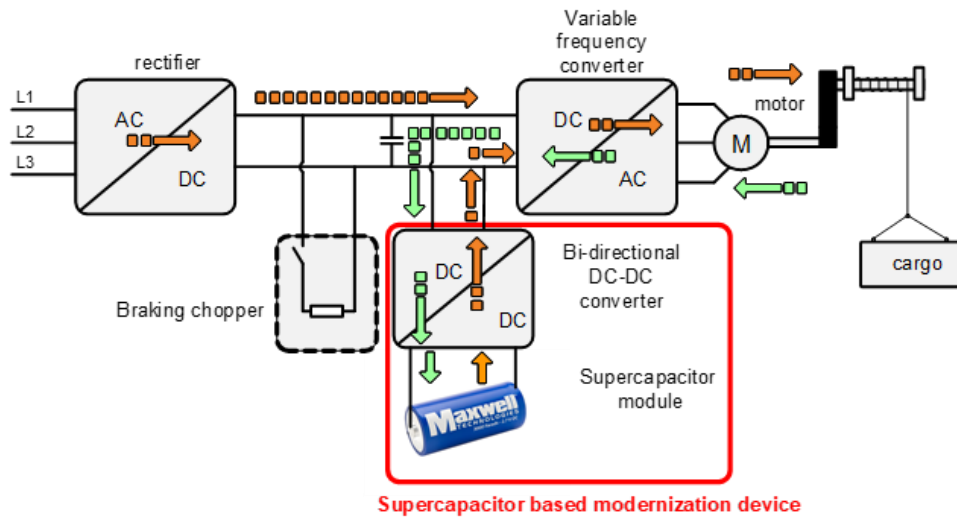


Fig. 1.1. Application of supercapacitor based modernization device in cranes.

The users are interested that such device payback period is as short as possible, to calculate this, it is important to know the lost energy. The simulation of container cranes is provided to calculate the energy lost in braking resistors. Most of containers in Latvia are transshipped in “Baltic Container Terminal” Ltd, so the cranes of this terminal will be considered in the calculation. This terminal has two cranes that lift cargo containers from the ship ashore and vice versa. Such a crane can lift a container 32 m above ground, the horizontal movement is 36 m. As an example of the cargo vessel container ship “Navi Baltic” is used. In calculations typical size, average mass of container, and the count of transshipped containers during the year are used. As the volume of containers handled is large – several hundred thousand containers, the mathematical statistical laws should be true when looking at all possible container loading/unloading profiles, and number of loading times corresponding to the handled containers.

By using Matlab software, it is calculated that 115 MWh of electrical energy are necessary to lift all containers during one year. If each of the cranes is equipped with the energy storage system consisting of 300 supercapacitors, energy consumption saving can be up to 40 %. The results shown in other research papers [7]–[12] show similar outcome. If both cranes are connected together via DC bus and one common energy storage is installed, more energy can be saved with less supercapacitors. Economic calculations show that supercapacitor based energy storage system paid back in five years.

2. Development of regenerative braking test bench to investigate energy recovery in electric transport

2.1. Development of regenerative braking test bench

During the movement of a vehicle the following forces act upon it (Fig. 2.1): the vehicle gravitational force that induces force R of reaction to the road, which determines the rolling resistance force F_R on the wheels, air resistance force F_A , and driving force F_D . To obtain the equations describing the movement of a vehicle, a simplified dynamic model was adopted [13]. The model is based on the assumption that the vehicle has mass m and equivalent moment of inertia J_{eq} corresponding to those of the driving wheels and all rotating parts cinematically connected to them. An expression of the vehicle deceleration during coasting as a function of speed can be obtained [14]:

$$-a = \frac{F_D + F_R + F_A}{m} = C_0 + C_1v + C_2v^2 \approx Cv. \quad (2.1)$$

Unknown constant C is estimated by using experimental data if launching a vehicle from a definite speed with the engine disengaged, and registering the current speed and distance during the free rolling until the vehicle stops. After the coefficients are obtained, the resistance momentum can be calculated [15]:

$$M_R = F_R r_w = -mar_w = mr_w (C_0 + C_1v + C_2v^2). \quad (2.2)$$

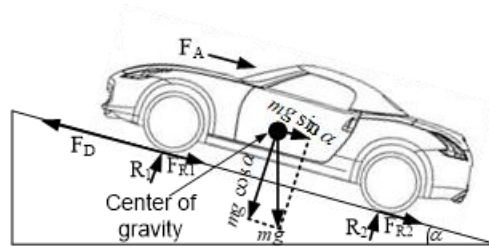


Fig. 2.1. Forces acting on a vehicle.

As load simulator for the traction drive the induction machine is selected as load emulator because of availability for further practical experiments on the test bench. The simulator of the vehicle traction drive's equivalent load is built by applying the induction motor with a field-oriented control frequency converter and a braking circuit containing a chopper-controlled braking resistor, the schematics is shown in Fig. 2.2. The AC drive motor generates the opposite load torque M_{AC} , which produces the total drive torque.

The torque of the DC motor with permanent magnets can be written as follows:

$$M_{DC} = K_D I_{DC}, \quad (2.3)$$

where K_D is a coefficient that depends on motor construction, and I_{DC} is the current of DC motor. The task for the control system of the load simulator is to control the frequency converter so that the AC motor acts like a rotating object with a very large moment of inertia J_{eq} and with equivalent

mechanical load torque M_{eq} . The desirable behavior of the mechanical system is described by the equation

$$\frac{d\omega}{dt} = \frac{K_D}{J_{eq}} I_{DC} - \frac{M_{eq}}{J_{eq}}, \quad (2.4)$$

where M_{eq} is the equivalent momentum of resistance.

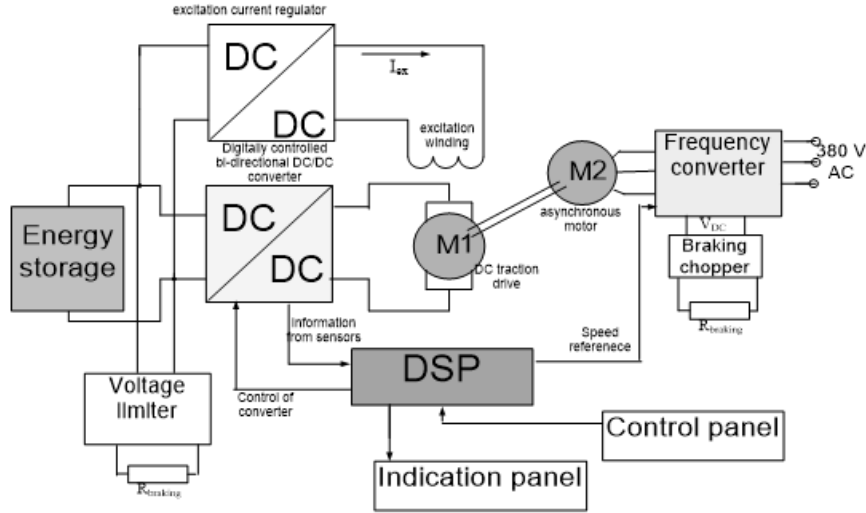


Fig. 2.2. Schematics of the test bench.

The expression for the reference angular speed of frequency converter could be obtained by integration of equation (2.4):

$$\omega_{ref} = \int (AI_{DC} - C\omega) dt. \quad (2.5)$$

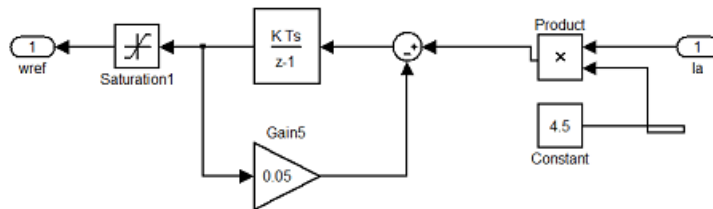


Fig. 2.3. Controller of the load simulator.

According to Equation (2.5), the controller of load simulator can be built as shown in Fig. 2.3. If the current of DC drive is larger than zero ($I_{DC} > 0$ A), the system provides acceleration, while at $I_{DC} < 0$ A the ω_{ref} value decreases and the system decelerates, thus imitating the braking mode. A more detailed description of the load simulator based on induction machine is available in [16], [17].

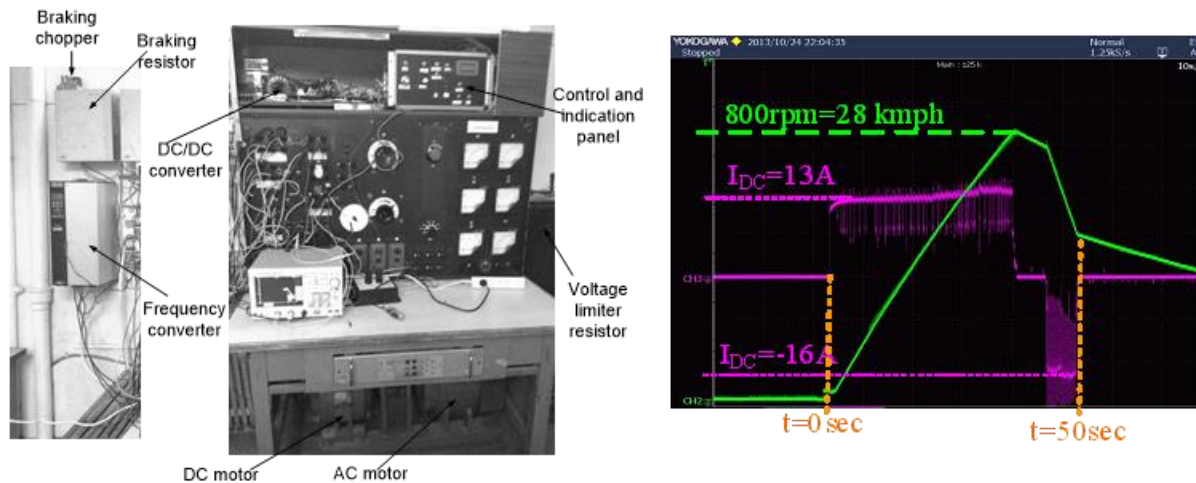


Fig. 2.4. The load simulator test bench and experimental results.

The bench contains a DC motor that simulates the electric vehicle traction drive and an AC induction motor simulating the traction drive load. The traction motor is connected to the energy storage that provides DC voltage through a two-quadrant/bi-directional digitally controlled DC-DC converter, which allows simulation of the traction and regeneration braking modes without reversing the direction of rotation. The AC drive motor generates load torque. Fig. 2.4 shows implementation of the digitally-controlled test bench for DC drive. The frequency converter is connected to the 380 V / 50 Hz network. When the DC motor is operating in the drive mode, the AC drive operates in the braking mode as the load, with the braking energy produced by the load simulator transferred to the braking resistor. In the braking mode of the traction drive model, the load simulator works in the motor mode. The control system of the load simulator is designed to work in the speed control mode. The DC motor used in the test bench has the following parameters: $P_{nom} = 3.7$ is nominal power, $R_a = 0.46 \Omega$ is the resistance of armature circuit, $n_{nom} = 1370$ rpm is nominal speed of the rotation. The AC motor is connected to the output of an FC300 type *Danfoss* frequency converter. In order to control the DC-DC converter and to send the reference value to the frequency converter, the STM32F407VGT6 microcontroller (MCU) is used.

The test bench can be used to emulate not only electric vehicles that have the same power as test bench but also to emulate a scaled operation of vehicles with higher power by using scaling. In Fig. 2.4 experimental results of emulating scaled model of tram are shown. The test bench that simulates the operation of tram is very useful for testing the supercapacitor based braking energy recovery system at first stages. Although the platform has lower power as compared with the real tram, the charging/discharging strategies of the energy storage and the topology of DC-DC converter can be tested successfully.

2.2. Development of supercapacitor based modernization device for lead-acid powered light electric vehicle retrofit

DC motors are still used in the drive system of light electric vehicles (LEV), especially, in small power range. These motors provide simple and cheap drive design necessary for low budget LEVs. The other DC motor advantage is direct and easy speed and torque control methods, which could be provided by help of simple dedicated traction controllers [18]. The speed is proportional to armature voltage of the motor while the torque is proportional to the supplied current. However, DC motors

have their drawbacks, which include high maintenance costs due to the commutator and brushes, which will wear in time, but due to rather simple DC brush motor traction drive solutions such cons are not significant at small power and low speed range for small passenger capacity LEVs, small LEV trucks and forklifts. But even if the LEV is equipped with an AC motor from the energetic processes at power supply side point of view there are no big differences, therefore it is possible to use DC motor as an object of the analysis of the additional storage system by any electric drive system.

The performance of the LEV is limited by the traction accumulator battery because of its high cost, maintenance needs, and limited lifetime. To achieve low cost and save power, the lead-acid battery of LEVs is the only economically efficient solution, but the lifetime of such battery is significantly reduced by high consumed current. The power demand profile for small LEVs is practically close to the city driving cycle and is characterized by repeated acceleration and deceleration, which will deteriorate the battery, especially when the battery state of charge is low [19], [20].

During deceleration, the traction drive produces short time high current peaks, which cannot be stored in the traction battery due to the low battery charging current value in comparison to discharge current. On the other hand, high charging current could be easily absorbed by supercapacitors, which are nowadays used in traction drive systems as well as in grid connected applications [21], [22]. For reducing of battery discharge current and regenerative braking energy storage, the LEV battery could be combined with supercapacitor based energy storage system (ESS). Supercapacitors are well suited to handle a peak power load, because they have low losses, long lifetime and are maintenance free compared to the batteries.

The research presented in this chapter is based on the approach that supercapacitor based modernization device can be connected to any common commercial LEV (taking into account voltage and power of the battery) via 2 wires to the DC bus and DC current clamp on the battery positive cable in the way that no reprogramming or modification of the existing drive is required [23]. Such ESS improves battery lifetime and stores regenerative braking energy.

Light electric vehicles today are used everywhere: in agricultural sector, tourism industry, warehouses, etc. Mostly LEV use a series connection of standard lead-acid batteries to run an electric DC motor. The voltage of the battery bank can be equal to 36 V, 48 V or 72 V. In the Thesis, the golf cart with nominal voltage equal to 72 V is selected for analysis as an example in the simulation model. The mass of the LEV used in the simulation is approximately equal to 1300 kg, the gear ratio is equal to $k_{red} = 8$, and wheel diameter is $D_{wheel} = 0.63$ m, maximum acceleration at nominal power is 2 m/s^2 [24].

During acceleration of the vehicle, the required amount of energy from the capacitor and the battery pack is transferred to the traction drive. During deceleration phase, the energy from the traction motor in generation mode flows to the supercapacitor or/and voltage limiter circuit. The charging current of the lead acid batteries is relatively small, therefore, the supercapacitor based ESS allows to store regenerative braking energy and decrease power spikes from the lead-acid battery. To utilize regenerative energy as much as possible, an advanced control strategy is required.

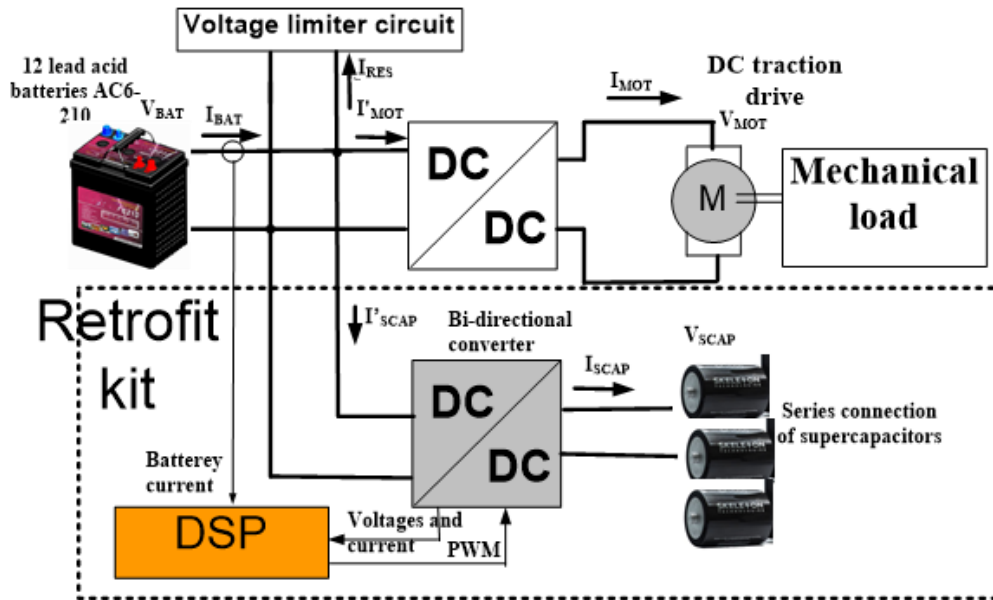


Fig. 2.5. Block diagram of the system [25].

The system (Fig. 2.5) that will be analyzed in the simulations contains a permanent magnet brush-type DC motor of the electric vehicle traction drive. The rated current of the motor is 150 A, voltage constant of the motor is equal to 0.1 V/rpm, torque constant is equal to 0.2, and rated speed is equal to 3000 rpm. The traction motor is connected to the hybrid system of energy storages that provides DC voltage through a DC-DC converter.

The LEV equipped with energy storage system modernization device to retrofit existing storage system, shown in Fig. 2.5 consists of the main battery, which has 12 lead-acid batteries with the capacity of 210 Ah in series, series connection of 33 Skelcap supercapacitors SC1500 with capacity 1500 F, internal resistance 0.079 m Ω , and bi-directional buck boost converter, which connects supercapacitor based ESS to the DC bus. The voltage limiter circuit restricts the DC bus voltage to 87 V. Such a system will be simulated in Matlab software. Mechanical load can be replaced by electrical machine that is controlled in such a way that it produces the same torque as real traction drive load.

To accumulate all regenerative energy, control algorithm of the supercapacitor based ESS that regulates voltage on the DC bus equal to 80 V can be used. An internal resistance of the lead-acid battery is 20 m Ω but of the supercapacitor bank – only 2.6 m Ω . The ratio at which the loss in both resistances is equal, can be found analytically or by using simulations. This control strategy would be the best to reduce losses. Additionally, there are losses in the DC-DC converter, and the energy of supercapacitor based ESS is less than of lead-acid battery, so theoretical proportion will lead to fast discharge of the ESS. Therefore, it is useful to regulate this proportion by software optimization to supply energy to the drive system in most efficient way.

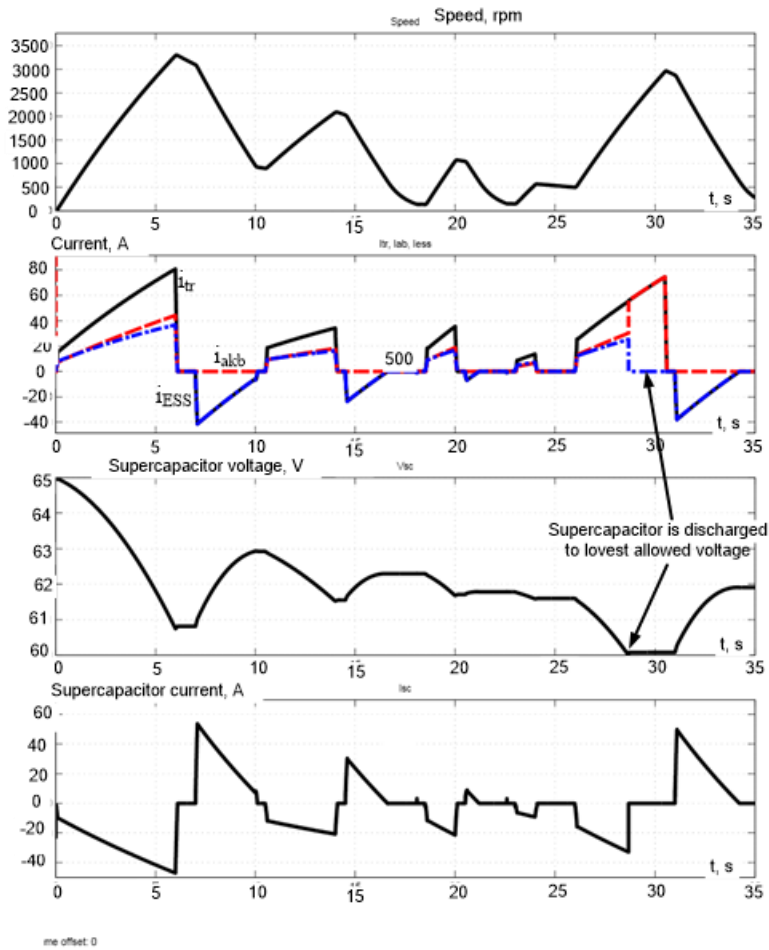


Fig. 2.6. Waveforms of currents and voltages using the ESS converter proportional control algorithm.

Fig. 2.6 shows the results of the simulation. In the simulation shown in the figure the proportion between both currents is shared almost equally, but, anyway in one period the supercapacitor based ESS is discharged to minimum voltage and all current is taken from the lead-acid battery, thus decreasing the efficiency. Of course, if acceleration time is very long, driving up the hill the ESS will be discharged to the lowest threshold anyway. The following two voltages and two currents were measured for the ESS control purposes: filter capacitor voltage V_f , supercapacitor voltage V_C , supercapacitor current I_C , and battery output current I_{BAT} . Three of these sensors can be placed inside the modernization device, and only the battery current sensor of a LEV should be installed outside the device. The battery current I_{BAT} is measured and used as a reference for the supercapacitor current controller.

The main task of the control system is to provide storing as much as possible braking energy of the LEV not allowing its dissipation in a braking rheostat, at the same time ESS must provide as efficient as possible discharge process. It means that the time in which power is supplied only from the lead-acid battery must be as short as possible. As shown in Fig. 2.6 the variable that reports about too low or too high proportional coefficient is voltage of the supercapacitors. If the voltage of supercapacitors stays equal to maximum voltage level for some time, more current must be taken from the supercapacitor ESS. If the voltage of the supercapacitor stays on the minimum allowed

voltage, more current from the battery must be taken. During the operation of vehicle, these periods of time can be measured and a new proportional coefficient calculated.

The possibility to implement such control algorithm on the real LEV and the control algorithm was tested in the laboratory. The load simulator of the vehicle traction drive, described above, is used to emulate the load of a real LEV. Fig. 2.7 shows the implementation of the digitally-controlled test bench and modernization device test platform for DC drive. When the DC motor is operating in the drive mode, the AC drive operates in the braking mode as the load with braking energy produced by the load simulator transferred to the braking resistor. In the braking mode of the traction drive model, the load simulator works in a motor mode.

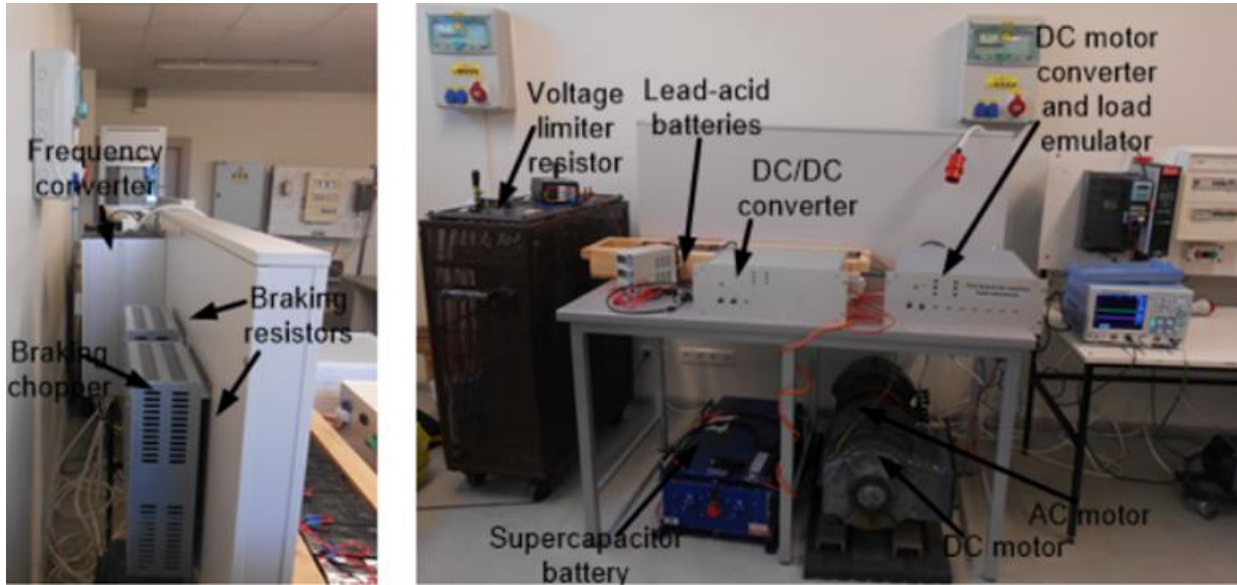


Fig. 2.7. Test bench used for supercapacitor based modernization device testing.

In the discharge mode, control system controls discharge current. The calculated value that is proportional to the battery current and the discharging current of supercapacitor current I_{SCAP} creates an error signal of the proportional-integrally-differential feedback system (Fig. 2.8). The reference value is corrected depending on supercapacitor voltage value. During acceleration, power is partly taken from the battery and ESS.

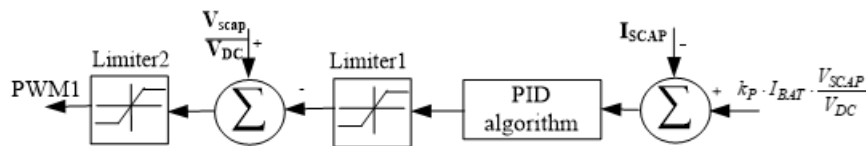


Fig. 2.8. Control system block diagram of the converter in boost (discharge) mode.

During the braking mode of the vehicle, the control algorithm should provide that all of the braking energy is stored in the supercapacitor based ESS, otherwise this energy is wasted in the brake resistor. To accumulate all regenerative energy, the algorithm, which is explained in Fig. 2.9 and keeps voltage on the DC bus equal to 120 V, is used, because the threshold of brake resistor operation is 125 V. Of course, the energy can be stored only in case if energy storage is not fully charged. If the duty cycle of a buck-boost converter is equal to the division of input voltage by output voltage, there is no current flow. To work in the buck mode, the duty cycle must be larger than this division, V_{scap}/V_{DC} is added to the value calculated by PI algorithm. Fig. 2.10 shows the

DC bus voltage during the braking phase. All of energy during braking is stored in the supercapacitor and voltage remains constant – equal to 120 V.

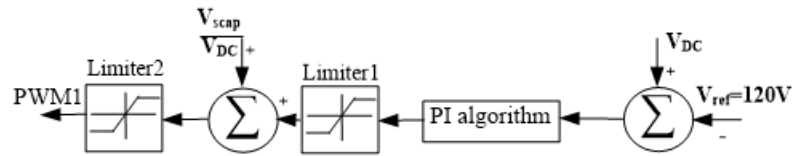


Fig. 2.9. Control system block diagram of the converter in buck (charge) mode.

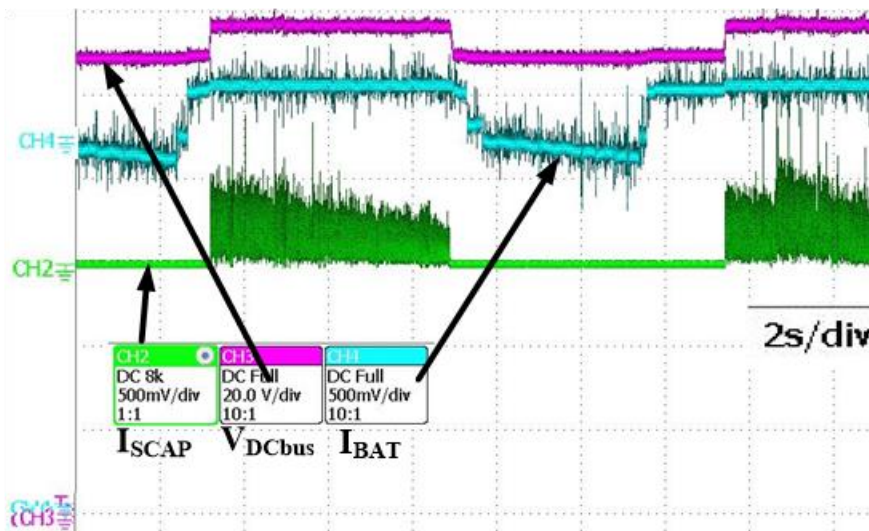


Fig. 2.10. Current and voltage of the proposed system in braking mode.

The theoretical and experimental results show that a supercapacitor based modernization device with an independent control system could be used for lead acid battery powered LEV efficiency and performance improvement without any modification of the existing commercial drive. Only two wires and the current sensor have to be connected, and the system can work by itself improving the efficiency of the drive system. Future research is needed to develop the ESS system without a battery current sensor. The supercapacitor based device with control system that supplies current proportional to the battery current is implemented in the laboratory test bench that emulates the real electrical processes of LEV. The experimental results show that the proposed control method can be implemented in the LEV drive system by using a microcontroller. Such modernization system allows storing regenerative braking energy of the vehicle, and the discharge process of supercapacitors has high efficiency.

3. Current ripple reduction by utilization of coupled inductors in high power density power electronics converters

The power electronics converter, which is installed in an electric vehicle should be as small as possible, therefore, it is important to investigate methods of increasing power density of the converter and in the same time increasing efficiency without significant increasing of costs. The utilization of multiphase converters becomes wider and wider. Equation (3.1) [26] shows the relationship between output current ripple ($\Delta i_{\text{two_phase}}$) of a two phase interleaved converter and current ripple ($\Delta i_{\text{single_phase}}$) of single phase converter. It shows, that by using an interleaved structure, the current ripple can be significantly reduced.

$$\frac{\Delta i_{\text{two_phase}}}{\Delta i_{\text{single_phase}}} = \begin{cases} \frac{2D-1}{1-D}, & \text{if } D > 0.5; \\ \frac{1-2D}{1-D}, & \text{if } D < 0.5. \end{cases} \quad (3.1)$$

Coupled inductor is a special form of multiple winding coupled magnetic structure. The advantages of integrated magnetic techniques are that the amount of core material is reduced [83]. The significant advantage of an interleaved converter with coupled inductor is that the ripple in one winding can be dumped to another phase [27]. The research on the interleaved DC-DC converters using a coupled inductor to reduce current ripples is reflected in [28]–[35].

3.1. Inversely coupled inductor for a two phase interleaved DC-DC converter

The interleaving structure has more inductors than the single phase converter. The two individual inductors of the two interleaving channels can be integrated on a single magnetic core to reduce the component size. The structure of an integrated inductor is shown in Fig. 3.1. Both windings of the inductors are built on the central leg of the E core. Although in literature [6] it is proposed to place the windings of the inductor on the wing legs thereby obtaining higher leakage inductance, manufactured coil formers for such a case are not available. The inductor, proposed in this Thesis, can be wound on ETD coil former in a convenient way as shown in Fig. 3.2.

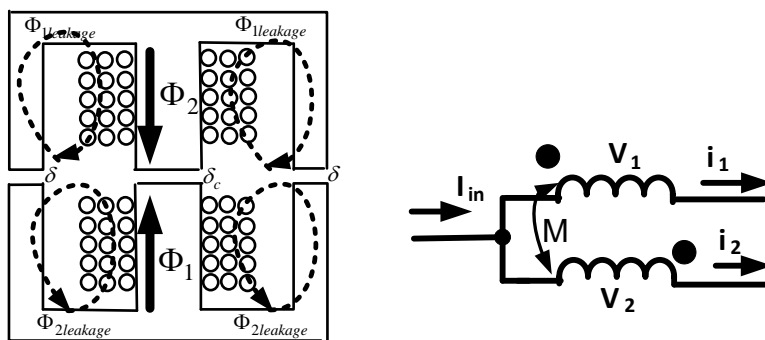


Fig. 3.1. Core structure of the coupled inductor and schematics of inversely coupled inductor [36].

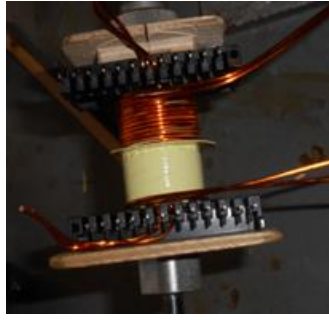


Fig. 3.2. Practical design of the coupled inductor [36].

The basic schematics of a two-phase coupled inductor is shown in Fig. 3.3. The mutual inductance M represents the coupling between the two inductors. The voltages across the two inductors (V_1, V_2) are related to the currents through them (i_1, i_2) as follows:

$$V_1 = L_1 \frac{di_1}{dt} - M \frac{di_2}{dt}, \quad (3.2)$$

$$V_2 = -M \frac{di_1}{dt} + L_2 \frac{di_2}{dt}. \quad (3.3)$$

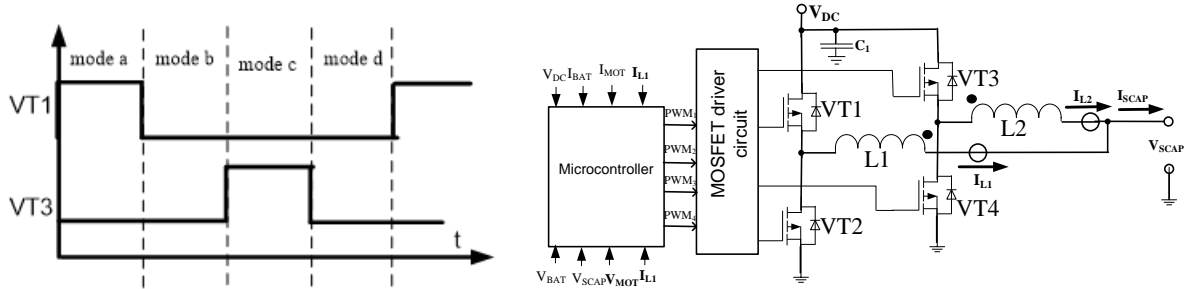


Fig. 3.3. Signals in one switching cycle and a circuit of two phase converter schematics.

In case of a two phase interleaved converter the control signals are shifted by 180° , Fig. 3.3 shows the gate signals of the transistors. The period can be divided into four different modes “a”–“d”. By solving (3.2) and (3.3) and taking into account the modes, the equivalent inductances can be calculated. The equivalent inductance during the period a is as follows [37]:

$$L_{eq1,a} = \frac{L - \frac{M^2}{L}}{1 - \frac{M}{L} \cdot \frac{D}{1-D}} = \frac{1-k^2}{1 - \left(k \frac{D}{(1-D)} \right)} L, \quad (3.4)$$

where k is the coefficient of coupling $k = M/L$.

$$L_{eq1,b} = \frac{L - \frac{M^2}{L}}{1 + \frac{M}{L}} = \left(\frac{1-k^2}{1+k} \right) L = (1-k)L. \quad (3.5)$$

$$L_{eq1,c} = \frac{L - \frac{M^2}{L}}{\left(1 + \frac{M}{L} \right) \frac{1-D}{D}} = \frac{1-k^2}{1 - \left(k \frac{1-D}{D} \right)} L. \quad (3.6)$$

The phase current ripples of phase 1 and phase 2 can be expressed with equations from the boost converter basics:

$$\Delta I_{1,a} = \frac{V_{in} D}{f_{sw} L_{eq1,a}} = \frac{V_{in} D}{f_{sw} L} \cdot \frac{(1-k) \frac{D}{1-D}}{1-k^2}. \quad (3.7)$$

$$\Delta I_{2,a} = \frac{(V_{in} - V_{out}) D}{f_{sw} L_{eq2,a}} = \frac{V_{in} D \left(1 - \frac{1}{1-D}\right)}{f_{sw} L_{eq2,a}} = \frac{V_{in} D \left(k - \frac{D}{1-D}\right)}{f_{sw} L(1-k^2)}. \quad (3.8)$$

The overall output current ripple is the sum of two phase current ripples and for inversely coupled inductors it is given as

$$\Delta I_a = \Delta I_{1,a} + \Delta I_{2,a} = \frac{V_{in} D}{f_{sw} L(1-k)} \cdot \frac{1-2D}{1-D}. \quad (3.9)$$

Equation (3.9) shows that the output current ripple will be larger in the case if inversely coupled inductor is used. Pulsations of current in each phase is determined by equivalent inductance $L_{eq1,a}$ if the duty cycle is less than 0.5, and $L_{eq1,c}$ if the duty cycle is more than 0.5, and will be less than in the case if conventional inductors are used. Using derivative functions equivalent inductance that minimize current ripple can be obtained:

$$\frac{L_{eq}}{L} = \frac{1-k^2}{1+ck}, \quad (3.10)$$

$$\frac{d\left(\frac{L_{eq}}{L}\right)}{dk} = \frac{-C\left(k^2 + \frac{2}{C}k + 1\right)}{1-Ck^2} = 0, \quad (3.11)$$

where $C = -\frac{1-D}{D}$ if $D > 0.5$ and $C = -\frac{D}{1-D}$ if $D < 0.5$. Solution of the expression $k^2 + \frac{2}{C}k + 1 = 0$ is given as:

$$k_{1,2} = \frac{-\frac{2}{C} \pm \sqrt{\frac{4}{C^2} - 4}}{2} = -\frac{1}{C} \pm \sqrt{\frac{1}{C^2} - 1}. \quad (3.12)$$

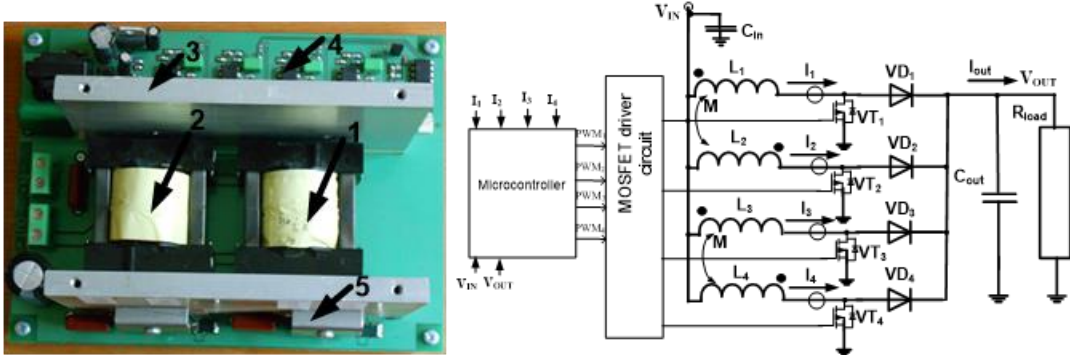


Fig. 3.4. Hardware implementation of DC-DC converter with two coupled inductors.

To validate theoretical analysis for phase DC-DC converter, it is designed with a nominal power of 2 kW (Fig. 3.4). Inductor is wound on ETD39 coil formers, its structure is shown in Fig. 3.2. All air gaps are selected equal to 1.5 mm, the count of windings is 30, the measured inductance is $L = 155 \mu\text{H}$, coupling coefficient $k = 0.7$. The experimental measurements coincide with theoretical results.

3.2. Current ripple reducing by using a coupled inductor in multiphase interleaved converters

To reduce per-phase current ripple even more, the multiphase interleaved converter structure can be used. Application of two phase coupled inductors to maintain energy transfer between all phases is proposed in the DC-DC converter shown in Fig. 3.5. The transistors VT_1 to VT_8 are controlled by pulse width modulation. Each parallel pair of switches turns ON with a signal shifted by 90° . To control this DC-DC converter, digital control will be used. Such converter can be used for many other applications, it can be modified as only buck or boost converter, because the synchronous rectification has better efficiency than use of the diodes.

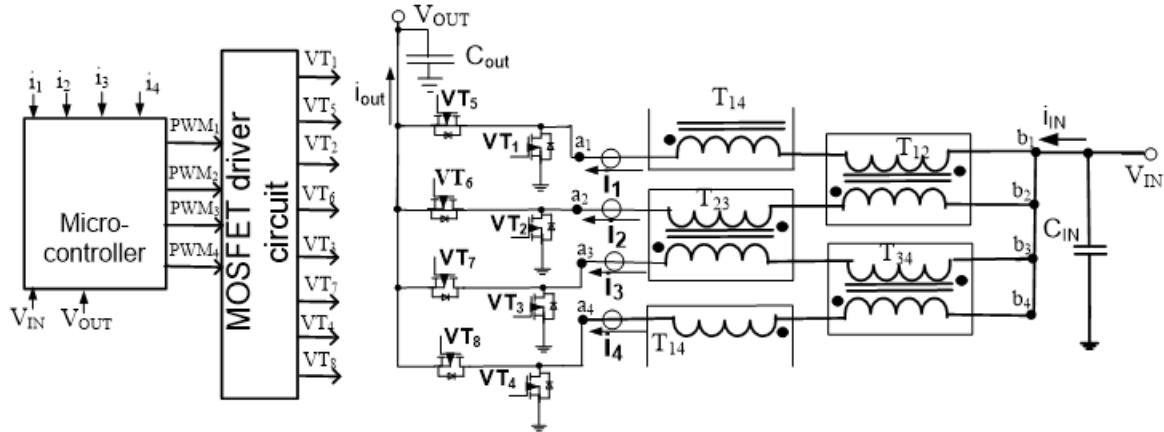


Fig. 3.5. The schematics of the interleaved 4-phase DC-DC converter with coupled inductors.

According to pulse length, there are four operation modes on a 4-phase interleaved converter with integrated magnetics. The first mode appears when the duty cycle (D) is less than or equal to $1/4$ of the switching period (T). The second mode appears when the D is between $T/4$ and $T/2$, and the third mode appears when the duty cycle is between $T/2$ and $3T/4$, and the fourth – when D is more than $3T/4$. The equations of this described circuit are solved analytically taking into account all these modes as described above.

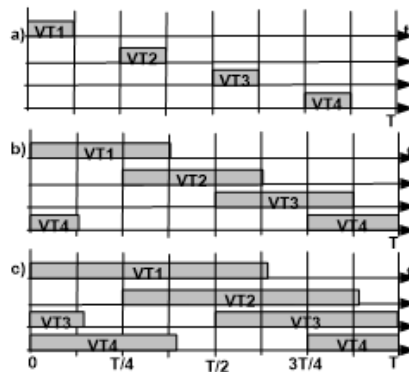


Fig. 3.6. Operation modes of an interleaved DC-DC converter.

An expression for input current ripple is obtained for the first period

$$\Delta I_{in(D \leq 0,25)} = - \int_{\frac{b-1}{b}T}^{\frac{T}{4}} \frac{4V_{IN}(1-b)}{2L-2M} dt = \frac{-\left(\frac{-3b+4}{4b}\right)(1-b)4V_{IN}T}{2L-2M} = \frac{(4-3b)(b-1)V_{IN}T}{b(2L-2M)}. \quad (3.13)$$

and for other modes, a more detailed analysis is available in [37]. By using these equations it is possible to draw graphs shown in Figs. 3.7 and 3.8. These graphs can be very useful to select the coupling coefficient and inductor value. Figure 3.8 shows that the coupling coefficient which is bigger than 0.9 causes significant input current ripple and therefore in this case this coefficient will be considered as maximum possible from the current ripple point of view. In the same way current ripple depends on the boost ratio. In the particular case boost ratio will be from 1.1 to 1.7, so the impact in this range is not so big.

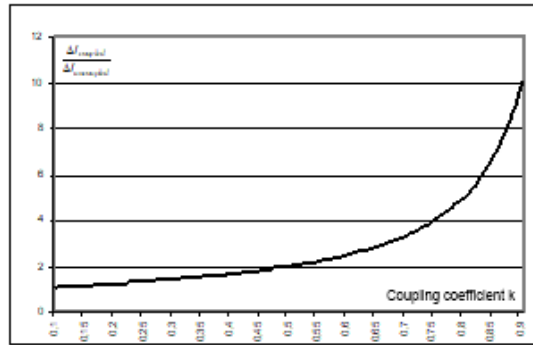


Fig. 3.7. Input current ripple according to coupling coefficient.

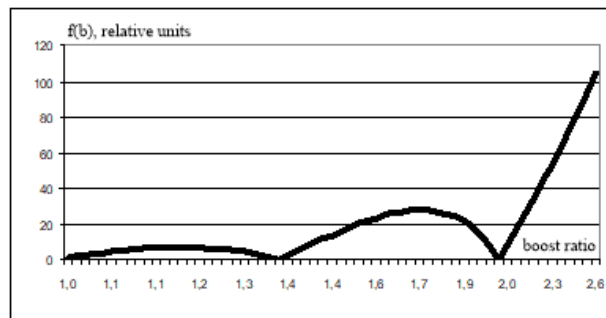


Fig. 3.8. Input current ripple according to boost ratio.

An experimental prototype was used to verify the analytical expressions. In the particular case, the inductor is wound on ETD59 coil former, its structure is shown in Fig. 3.2. The central air gap and air gaps of outer legs are selected equal to $\delta = \delta_c = 0.5$ mm, the number of windings is 30, the measured inductance is $L = 400 \mu\text{H}$, coupling coefficient $k = 0.85$. There are two inductors in series in each phase. It means that the inductance is almost 2 times larger than in the case of an uncoupled inductor and output current ripple is only three times larger than in the case of the uncoupled inductor. Per-phase current ripple is reduced at least 2 times. The external view of the prototype is shown in Fig. 3.9. In order to control the DC-DC converter, the STM32F407VGT6 microcontroller (MCU) is used. The current of each phase is measured by low cost ACS713 Hall effect based current sensor, and PI control algorithm is controlled by pulse width modulation (PWM). The PWM signals shifted in phase by 90° control IRFP4768 MOSFET transistors.

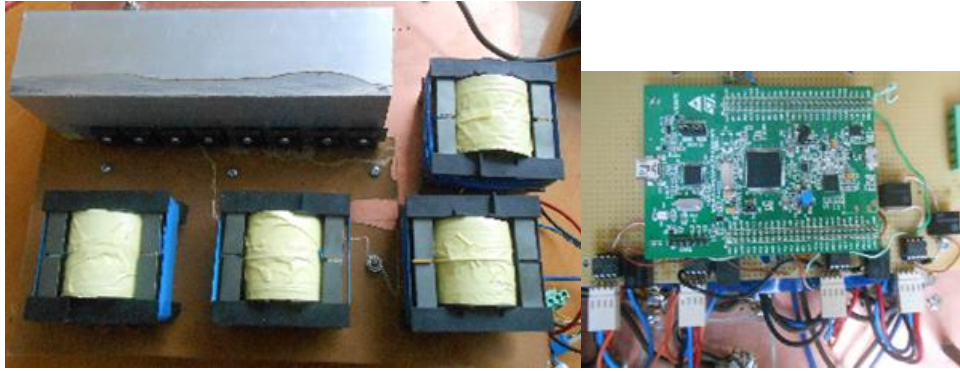


Fig. 3.9. Prototype of a four phase DC-DC converter with coupled inductors.

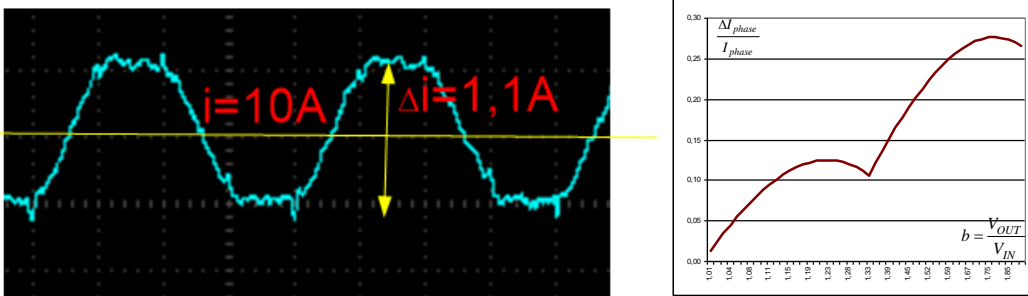


Fig. 3.10. Per-phase current waveform at duty cycle 0.25 and measured per-phase current ripple as a function of duty cycle.

Fig. 3.10 shows that the per-phase current ripple is lower than 30 % of per-phase current in the case of uncoupled inductor. The main disadvantages of such converter are increased costs and the need to regulate current in each phase.

3.3. Application of directly and inversely coupled inductor combination in DC-DC converters

The 4-phase interleaved DC-DC converter with integrated magnetic component and auxiliary inductor is shown in Fig. 3.11. In this figure, V_{in} and V_{out} are the input and output voltages, I_1 , I_2 , I_3 and I_4 are the inductor currents of each phase, and I_{IN} and I_{OUT} are the input and output currents. The MOSFETs are switched with a phase shift of 180° . Integrated magnetic components are applied in the converter to reduce the volume, weight, and cost of the magnetic components. The windings of the first and second phases are separated by isolating material and placed on the coil former. The windings are made of litz-wire. The number of windings is equal to 5, and air gap is 0.1 mm. The inductance is 16 μH , and coupling coefficient is 0.72.

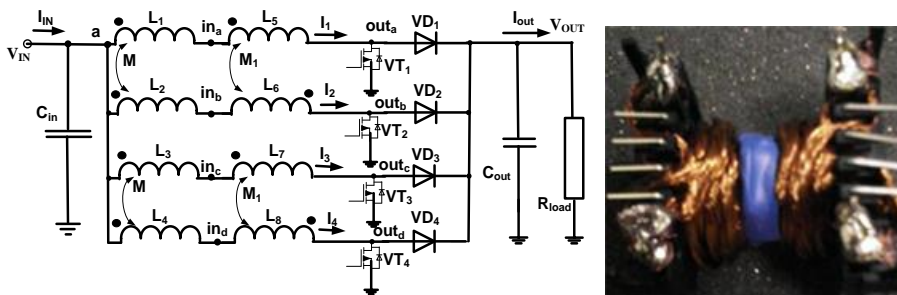


Fig. 3.11. Four-phase interleaved boost converter with inversely and directly connected coupled inductors, and the construction of such inductor.

In this case, ferrite core with air gap is used to design this inductor. The disadvantage of ferrite is low B_{SAT} , and to overcome this, the air gap in the core must be introduced. With a large air gap, the leakage flux through the air affects directly the windings which are closer to the air gap inducing a current which is opposite to the main current – it is called fringing effect and is described in detail in [38]. In this case, to minimize this effect, the windings are moved away from the air gap. Figure 3.12 shows the simulation of magnetic field of the inductor by using FEMM 4.2 finite element method magnetic field simulation software. As can be seen, only small part of the fringing flux crosses the windings. Directly coupled inductor is compared to conventional inductor in this figure, as can be seen, the magnetic flux into directly coupled inductor is lower. Directly coupled inductor can be realized in a similar way as inversely coupled inductor, but windings are connected in a way to create magnetic flux in one direction. The inductor has two windings in the central leg of the E-E cores. The magnetic structure is very similar as in the case of inversely coupled inductor only with a larger air gap to avoid saturation of the core.

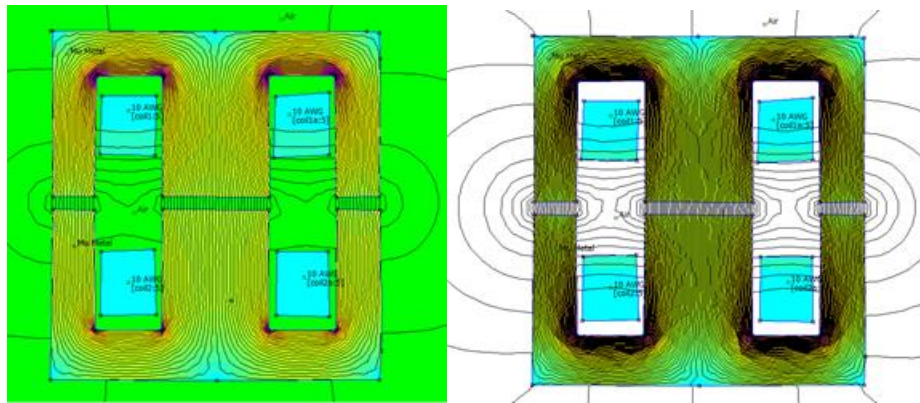


Fig. 3.12. Magnetic field of directly coupled inductor and conventional inductor.

More detailed analysis and comparison with using of conventional inductor is given in [39]. The main conclusion is that the increasing of coupling coefficient leads to a significant current ripple of output current, therefore, a compromise must be found between the current ripple and flux density. In the case of directly coupled inductor the flux density is smaller and, therefore, the inductor can be more compact and with lower losses.

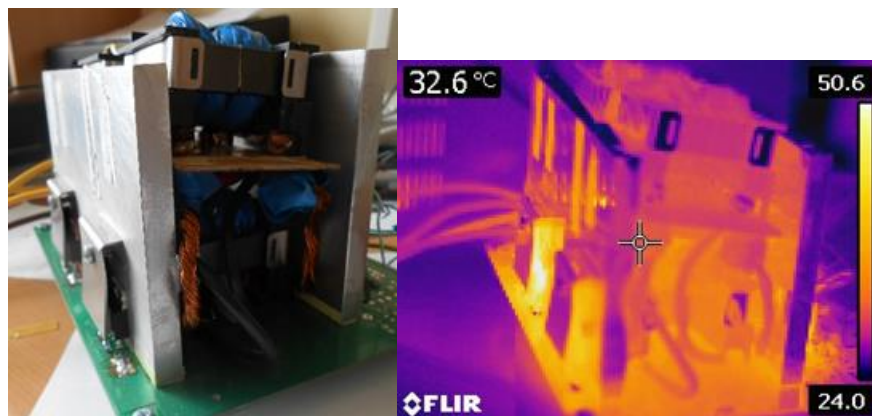


Fig. 3.13. Prototype of a four phase DC-DC converter and thermal image.

To verify theoretical expressions and test benefits, a prototype with a combination of directly and inversely coupled inductors (Fig. 3.13) has been developed. The pulse width modulation (PWM) signals are shifted in phase by 90° . Inversely coupled inductor and directly coupled inductor are wound on ETD39 coil formers. The number of windings of both kinds of inductors is equal to 5 in each phase, summary coupling coefficient is equal to 0.3, so to reduce per-phase current ripple also a close coupled inductor can be used with smaller size, but then a directly coupled inductor must be bigger and with higher inductance.

The results show that the use of directly coupled inductor can be considered as a possible solution not only for overall input current ripple minimization but also for per-phase current ripple reduction. The creating of directly coupled inductor is more complicated than additional single phase inductor. The experimental results match with the theoretical ones, and it can be concluded that the integration of the magnetic core of inductors allows to reduce per-phase current ripple and the size of the magnetic components.

4. Modernization device for the improvement of ICE starting

To make internal combustion engine (ICE) starts it should be turned at a certain speed, so that it sucks fuel and air into the cylinders and compresses it. Usually the starting system converts electrical energy from the lead-acid batteries into mechanical energy to turn the engine. The improvement of the starting system with supercapacitor allows the use of old batteries, which are unable to provide enough power to start the ICE but have energy to charge supercapacitor with low current. It reduces high discharge currents from lead-acid battery thus prolonging the lifetime of the lead-acid battery 2–3 times [40]. Some forecasts expect that the start-stop system that allows switching off the ICE during the short time stops will be included in more than half of new ICE vehicles. In such system, lead-acid starter batteries that enable the system to restart the engine many times per day may need to be replaced more frequently, therefore, the demand for new technology that solves this problem is high. Moreover, battery-supercapacitor hybrid reduces the volume of the storage device by 30 % and reduces weight by 25–40 % [41], [42].

The battery-supercapacitor hybrid can be passive [43], semi active [44], and fully active [45], [46]. In the passive topology, the lead-acid battery and supercapacitor are connected parallelly without any converter. Although this hybrid is the cheapest, the whole energy of the supercapacitor cannot be used. The fully active topology attains the best performance and often is used in hybrid cars, but in this case it requires bulky, expensive DC-DC converter for high current. This chapter presents the approach based on low power DC-DC converter used for charging of the supercapacitor and active high current switch.

4.1. The starting process of an ICE

To study ICE starting process, a hall-effect based current sensor HTFS 200-P with maximum current of 300 A and Fluke 199C oscilloscope were used. The measurements were performed on two passenger cars – Skoda Octavia with 1.8 petrol engine and Toyota Corolla with 2.0 diesel engine. Fig. 4.1. shows typical current and voltage profile of the starting process. The current is higher in the case of diesel engine, if the ambient temperature is lower, in the same way engine type, starter motor type, maintenance conditions, oil viscosity, ignition quality, and other factors affect the starting current, but, anyway, current profile trend stays similar to that shown in Fig. 4.1. The characteristic starter operation modes are short circuit mode in which rotation speed of the starter motor is close to zero, the current and torque is maximum, and the load mode in which the engine starts to rotate and the current decreases. The period with high current lasts about 50 ms. The ripples in the current are due to the compression and expansion of the engine pistons.

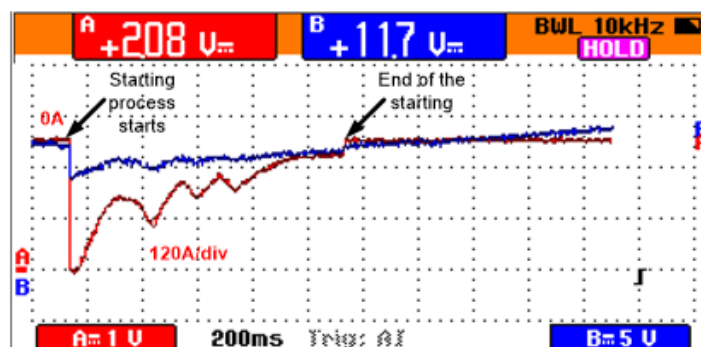


Fig. 4.1. Typical current and voltage profile of the starting process.

To start an ICE, the motor must be accelerated to speed ω_0 , in such a case back electromotive force E_0 can be calculated as follows [47]:

$$i_{L0} = \frac{V_B - E_0}{R_{Bat} + R_S}, \quad (4.1)$$

where V_B is no load voltage of the battery, E is the back electromotive force, R_S is the stator resistance, R_{Bat} is internal resistance of the battery, and i_L is the start current. From (4.1) it can be concluded that, if the state of charge or state of health of lead-acid battery is low, then V_B is low but R_{Bat} larger than usual, therefore, current i_{L0} can be too small for developing sufficient torque to overcome load torque for accelerating engine to the start speed ω_0 . Such battery is not valid for ICE starting and must be charged or replaced. The very high short circuit current in the first moment of the starting process drastically affects state of the health of the batteries as lead acid batteries operate best at constant power levels. Reducing this spike from the battery in a starting circuit can increase the life of the battery, because the stress on it will be less as the starter is first engaged. The overcurrent during short circuit mode of the starter motor causes a significant drop of the battery voltage. This voltage drop can generate the malfunction of the devices connected to the battery. Fig. 4.1 shows the battery voltage during the starting process in summer with charged battery but anyway the voltage drops below 9 V (the normal limit). The problem of the voltage drop during starting is more important in vehicles with the start stop function while the frequency of engine start is much higher than in conventional cars and could endanger the users by resetting systems that must be uninterruptible. One of the solutions to prevent the voltage drop is to use two batteries [48]: one to start the engine and the other for the supply of the electrical systems. The proposed device allows to stabilize the battery voltage during short circuit mode.

4.2. Supercapacitor based modernization device to improve ICE starting

The proposed system for ICE starting is based on series connection of supercapacitors and the DC-DC converter (Fig. 4.2). The supercapacitor based energy storage is charged by using the converter with low current. During the ICE starting process, energy is taken from the supercapacitors, as a result the lead-acid battery is not damaged by short circuit current, which increases lifetime of the battery, and the supply voltage of the vehicle electronics stays constant during the starting process.

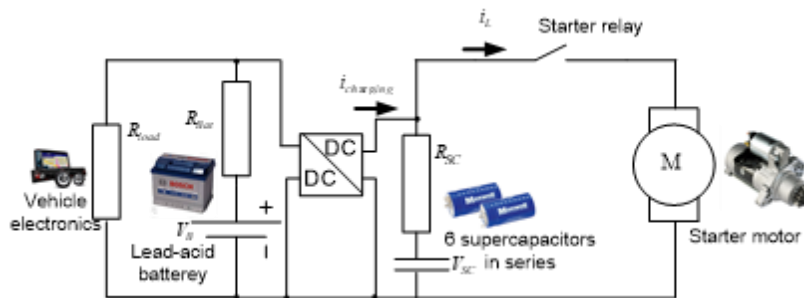


Fig. 4.2. Schematics of the proposed ICE starting system.

BCAP0350 E270 T11 supercapacitors are selected as energy storage for the device. In the datasheet, the maximum internal resistance is specified and is equal to 3.2 m Ω . To test modernization device integration in the starting system, a prototype was developed to test it during the ICE starting process. Fig. 4.3 shows the prototype of the device, it has a size of

150 mm × 110 mm × 8mm. The prototype was installed on the vehicle and tested for a month, no problems were indicated in the operation. With one charging of supercapacitors the ICE can be started 2–4 times, but the test was performed in summer and with vehicle equipped with petrol engine. The energy stored in supercapacitors is too little to start ICE in any conditions. Such engine start module has enough energy only for petrol cars with small ICE. Fig. 4.4 shows voltage of the supercapacitor battery and the current during the starting process. Fig. 4.4 shows that the voltage of supercapacitor decreases fast, it means that the energy of supercapacitors is consumed to start ICE and in low ambient temperature the energy will be consumed so fast that starting of the ICE becomes impossible. Therefore, further improvements of the device are proposed.



Fig. 4.3. Prototype of modernization device for starting ICE.

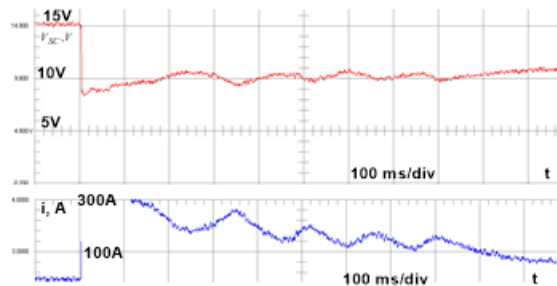


Fig. 4.4. Voltage of supercapacitors and current during starting the ICE.

4.3. Modernization device for ICE starting with active control

As supercapacitors with higher capacity significantly increase the costs of the system, it is necessary to find a way to remove current spikes from lead-acid battery. The MOSFET transistors with low breakdown voltage are cheap and with low on-state resistance. The parallel connection of several MOSFETs can commutate the starting current for a short time without heating up. Fig. 4.5 shows an ICE starting system complemented with two controllable switches. The supercapacitors through MOSFET VT_{SC} are connected to the starter, but the lead-acid battery through VT_{BAT} is connected to the starter. When the starter relay closes the main contact, the switch VT_{SC} is turned on, short circuit current goes from the supercapacitor to the starter motor. After typical short circuit time (approximately equal to 150 ms) or by detecting recovery of the voltage switch VT_{SC} is turned off, and switch VT_{BAT} is turned on. The power to crank engine goes from the lead-acid battery in this state. From the voltage pulsations during cranking rotation the speed can be detected. If this speed is analyzed then there can be detected speed loss of the starter motor (internal resistance of lead acid battery is too high or voltage too low to start ICE) and VT_{SC} can be switched on to supply energy to the engine starting from both sources.

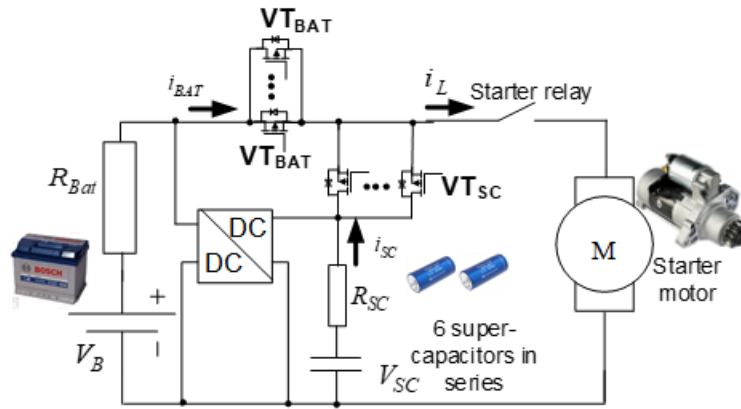


Fig. 4.5. ICE starting system with MOSFET switches.

The supercapacitors are charged through the DC-DC converter with low current. During the starting process of ICE, energy is taken partly from lead-acid battery and partly from supercapacitors. As a result, the lead-acid battery is not damaged by the high short circuit current, the lifetime of the battery increases and the supply voltage of the vehicle electronics stays more constant during the starting process, as the internal resistance of supercapacitors is lower and they can be charged to 15 V. Additional benefit of such a solution is the simple connection of the device in parallel to the lead-acid battery and limitation of generator current during the first moment after starting.

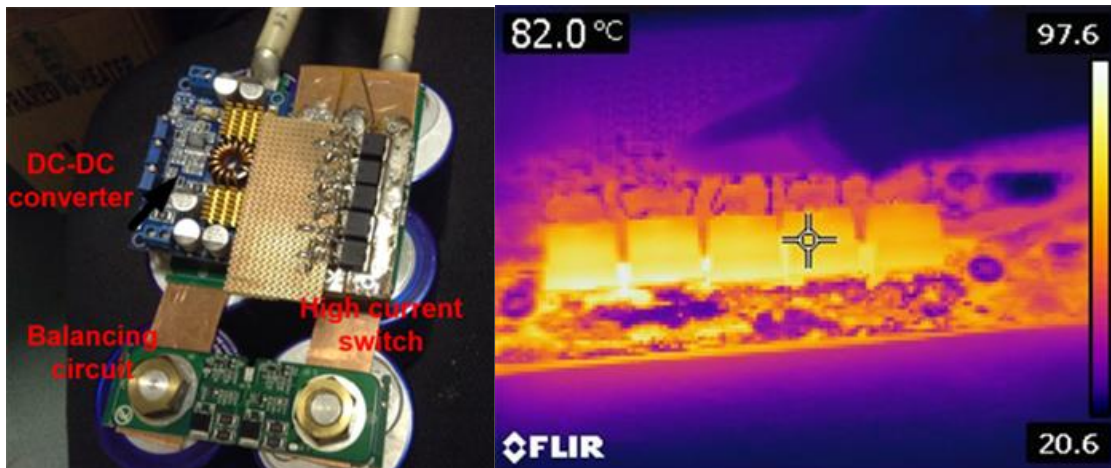


Fig. 4.6. The hardware of ICE start battery assistance device and temperature of the MOSFET based switch and of supercapacitors current during starting process.

For the practical application in cargo transport where start and stop is required often the prototype was developed with a series connection of 6 SAMWHA DH5U128W60074THT 1200 F supercapacitors. In the datasheet, only the maximum internal resistance is specified and is equal to 0.5 mΩ for one supercapacitor. Non-isolated buck-boost DC-DC converter was utilized to charge supercapacitor energy storage in current mode. Conventional passive balancing circuit is used to balance voltages of supercapacitors. The parts of hardware are shown in Fig. 4.6. The MOSFET transistors with low on-state resistance were selected and used as switches to connect supercapacitors.

The parallel connection of several MOSFETs can commutate starting current for short time without overheating as can be seen in Fig. 4.6. The high current from the lead-acid battery during

short circuit mode is eliminated from the other side. This current spike will be supplied from supercapacitors and can reach even higher value as the internal series resistance of supercapacitors is lower. To limit peak starting current from supercapacitors, MOSFET switching on in linear mode can be used, the starting process becomes only a bit longer, but the lifetime of the starter motor and supercapacitors is significantly increased. It will lead to additional heating of the transistors, therefore, the heatsink size, more likely, should be increased. Such approach allows to fully control the power flows, and there is a possibility to switch on and off the supercapacitors depending on the state of charge.

5. Development of modernization devices including DC-DC converters for frequency converter controlled electric drive retrofit to increase energy efficiency

In the recent years, storage of energy has become extremely important in renewable energy systems (such as wind energy [139], small hydroelectric power plants [49] and photovoltaic plants [50]) because the wind does not always blow and the sun does not always shine at any given location as well as in the regenerative braking systems. Therefore, energy storage can be regarded as an essential component of future energy systems that use large amounts of various renewable resources. The proposed solution is to integrate DC-DC converter together with supercapacitors into one module and retrofit the existing electrical drive system to increase energy efficiency and reliability during voltage outages. The central part of an energy storage system is the DC-DC converter, which connects the supercapacitor pack or the battery pack with the DC bus. A DC-DC converter is always required to allow energy exchange between the storage device and the rest of the system. Such a converter must have a bi-directional power flow capability with flexible control in all operating modes.

5.1. Multiphase bi-directional DC-DC converter for energy storage integration

5.1.1. Topology selection

Interleaving control schemes are widely used in the converter applications, for example, as voltage regulating modules [51], [52], in renewable energy generation [53], in traction drive systems [54], [55], and many other areas. Merits of such control methods are reduction of input/output current or voltage ripples and volume and increase in the processed power capacity of the converters. In the discontinuous conduction mode (DCM) the reverse-recovery losses of the diode are eliminated and switching losses can be reduced. Thus, body diode of the MOSFET transistor can be used. Compared to DCM with constant switching frequency [56], [57], variable frequency mode yields to lower total harmonic distortion of the current and smaller peak inductor currents and results in lower switching and conduction losses [58]. It is more difficult to realize interleaving features of a converter with variable frequency operation. The phase shifter based on IC even for two phase converter [59] is complicated, therefore digital control of the DC-DC converter is implemented. Thus, the converter can be easy and quickly configured for specific application.

The proposed interleaved bi-directional converter [60] (Fig. 5.1) has six phases and it is bi-directional as it can work in both buck and boost modes. If boost mode is selected, low side MOSFET transistors (with an even number VT_2-VT_{24}) are being switched on and off but the high-side transistors remain turned off (with an odd number VT_1-VT_{23}) and vice versa (Fig. 5.1). The body diode of the transistor is used as a freewheeling diode. If it is necessary to improve efficiency of the converter, parallel diode can be placed parallel to the MOSFET transistors or, preferably, synchronous rectification can be used. In the particular converter these options are not utilized to improve reliability of the converter, as by using the transformer based MOSFET driver situation when gate signal of the transistor stays open the whole period can be eliminated, faulty transition from buck mode to boost mode is prevented. In order to control converter, six analogue values are measured and converted into digital signals (Fig. 5.2).

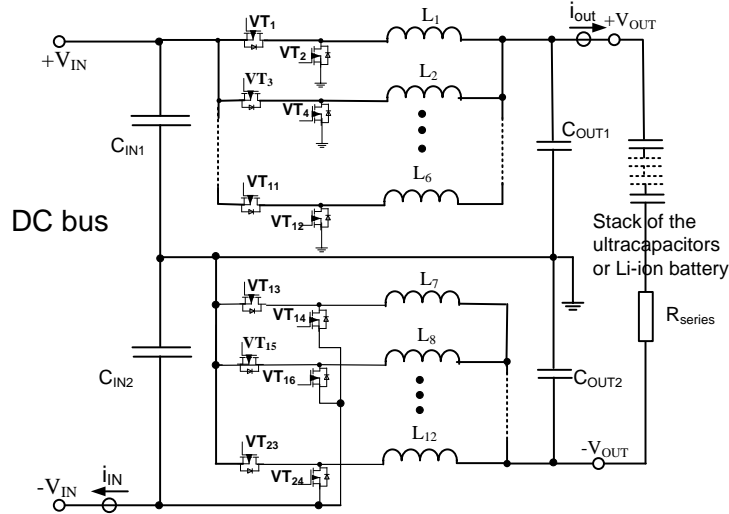


Fig. 5.1. Scheme of a bi-directional two level 6-phase DC-DC converter.

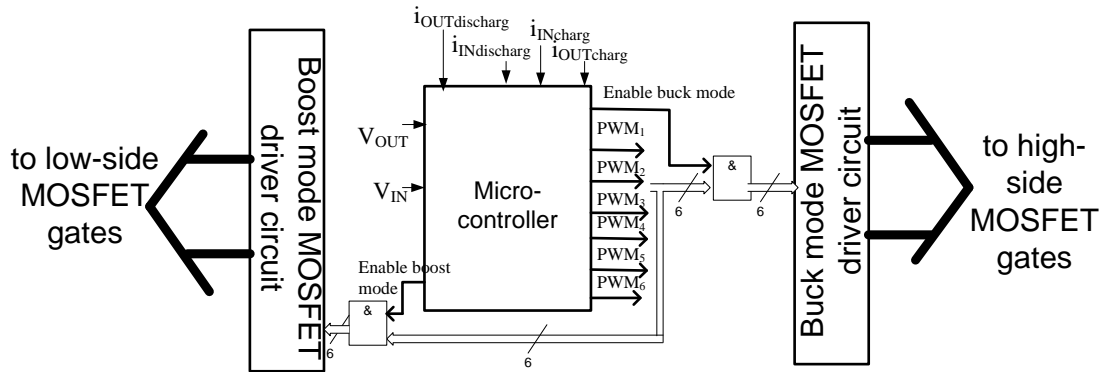


Fig. 5.2. The input and output signals of microcontroller.

The MOSFET transistors with the maximum voltage of 800 V are available on the market while the price of the high voltage SiC transistors is still very high and on-state resistance of MOSFETs with a lower breakdown voltage is significantly lower. This converter is provided to recover the braking energy of the AC drive and is installed on the DC bus of an inverter with maximum voltage of 750 V. To make using MOSFETs transistors for such voltage possible, two level structure of the converter is selected. This allows exploit even cheaper SPW52N50C3 560 V MOSFETs with significantly better parameters than 800V MOSFETs or IGBTs. In [61], [62] the number of levels is increased to improve the efficiency of the converter as low-voltage MOSFETs have better parameters. It is possible to develop a multilevel structure with the proposed control algorithm in a simple way. To prevent misbalance of the voltages of the capacitive divider, signals to the gates of the transistors of the corresponding phase must be equal. Therefore, a transformer based MOSFET driver with two secondary windings is applied.

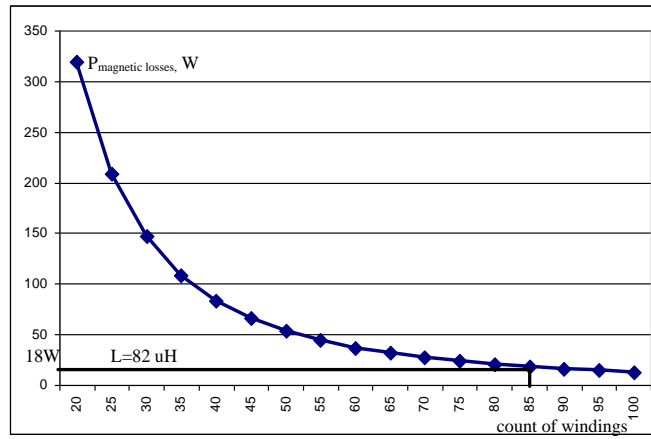


Fig. 5.3. Selection of the count of windings of the inductor.

High current flows through windings of the inductor in the DCM mode. As in this mode lower value of the inductance is necessary, the inductor is of a small size but a large air gap is necessary in comparison with the inductors for the CCM mode. If a large air gap is introduced in the core, the leakage flux through the air affects the windings, which are closer to this air gap, inducing current opposite to the main current (fringing field effect). Due to this effect iron powder toroid T300-2 with distributed air gap is selected although smaller losses can be achieved by using a ferrite core if fringing effect is eliminated (for example, as proposed in [5] or in [12]). Magnetic flux (B) and magnetic losses ($P_{\text{magnetic loss}}$) can be calculated as follows [63]:

$$B = \frac{V_{\text{average}}}{4fSw}, \quad (5.1)$$

$$P_{\text{magnetic_loss}} = \frac{f}{\frac{4 \cdot 10^9}{B^3} + \frac{3 \cdot 10^8}{B^{2.3}} + \frac{2,7 \cdot 10^6}{B^{1.65}}} + 8 \cdot 10^{-15} f^2 B^2, \quad (5.2)$$

where f is switching frequency, S is cross section area of the core, w is number of windings.

Using the equations mentioned above, it is possible to draw a graph shown in Fig. 5.3 that presents magnetic losses depending on the number of windings. From this graph, the minimum number of windings that allows reducing magnetic losses is selected. The inductance of such inductor is equal to 82 μH .

5.1.2. The control algorithm

In the DCM mode, per-phase current is determined in each period and it does not depend on the previous periods. This greatly improves the converter dynamics and simplifies the control system of the converter as in DCM mode converter with voltage sources in output and input even with open-loop regulation system with pulse-width modulator (PWM) is stable, while in the CCM mode the feedback (current sensor) in each phase is necessary.

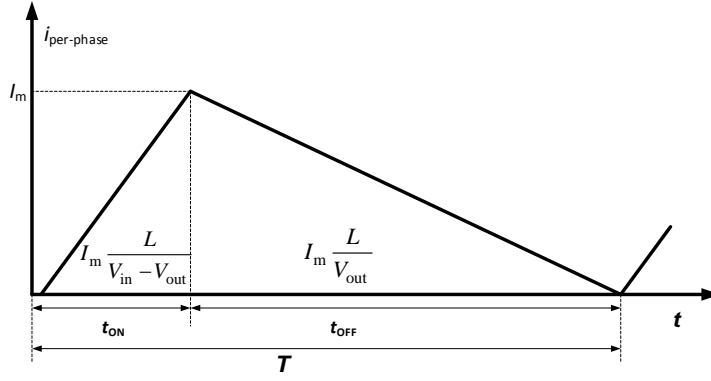


Fig. 5.4. Inductor current at boundary conduction mode in buck mode.

In boundary conduction mode (BCM), the peak current in the inductor is twice the average current. Therefore, this mode is the most economical and control will be designed to ensure work of the converter in DCM mode as close as possible to BCM mode. The summary output current I_{OUT} of n phase converter is the sum of all choke currents. In the BCM, the peak current in the choke (I_m) can be expressed as shown further.

$$I_m = \frac{2I_{OUT}}{n}. \quad (5.3)$$

The disadvantage of the BCM is a variable operating frequency, but it can be avoided by using digital control algorithms. Using the inductance (L) as well as the input (V_{in}) and output (V_{out}) voltage the required on-time (t_i) and off-time (t_p) for buck mode can be calculated as shown in (5.4) and (5.5) and similarly for boost mode to ensure operation in boundary conduction mode. Inductor current in BCM is shown in Fig. 5.4.

$$t_i = I_m \frac{L}{V_{in} - V_{out}}. \quad (5.4)$$

$$t_p = I_m \frac{L}{V_{out}}. \quad (5.5)$$

The variable I_m can be used not only to maintain the desirable output current but also to control input current and output voltage. This can be done if I_m is output of the proportional-integral (PI) regulator that is shown in Fig. 5.5 and can be calculated as shown in (5.6) where K_p is proportional coefficient, T_i is integral coefficient, t_{sample} is time between two samples, and DELTA is the difference between the reference value and the actual value of a controlled parameter. Of course, I_m must be limited to the maximum value allowed – in this case to 20 A. Power tracking can be carried out by using the open-loop control, thus current sensing in each phase is not necessary.

$$I_m(k) = DELTA(k) \cdot K_p + I_{m,i}(k-1) + DELTA(k) \frac{t_{sample}}{T_i}. \quad (5.6)$$

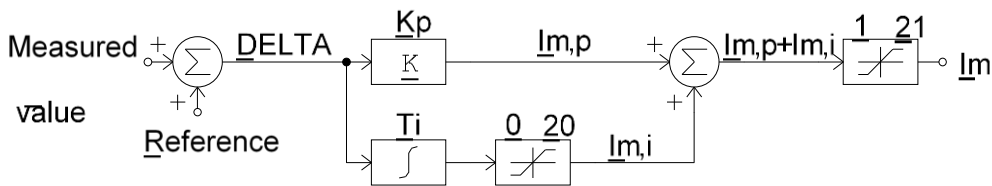


Fig. 5.5. Calculation of I_m by PI regulator.

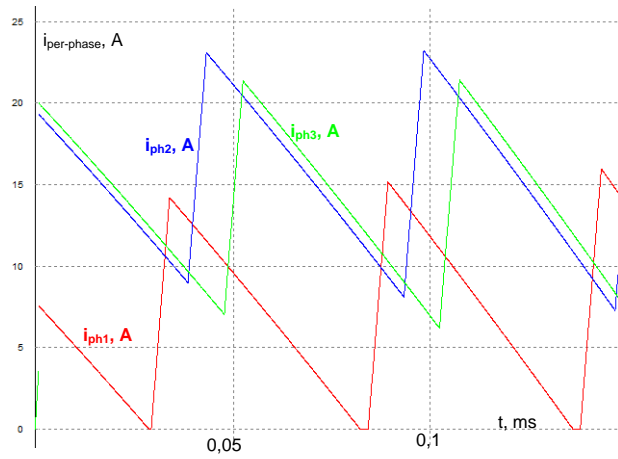


Fig. 5.6. The misbalance of the current in BCM due to unequal inductances.

An error in the voltage measurement or unequal inductance values can cause unwanted transition from the BCM into CCM for some of the phases (Fig. 5.6). In such case, entering into continuous conduction mode has to be avoided to prevent overcurrent. Therefore, it is beneficial to stay in DCM, which means that somewhat enlarged switching period is necessary. In order to obtain pulse length necessary to stay in the DCM, inductance in equation (5.4) and (5.5) is multiplied by the coefficient. The results are shown in Fig. 5.7.

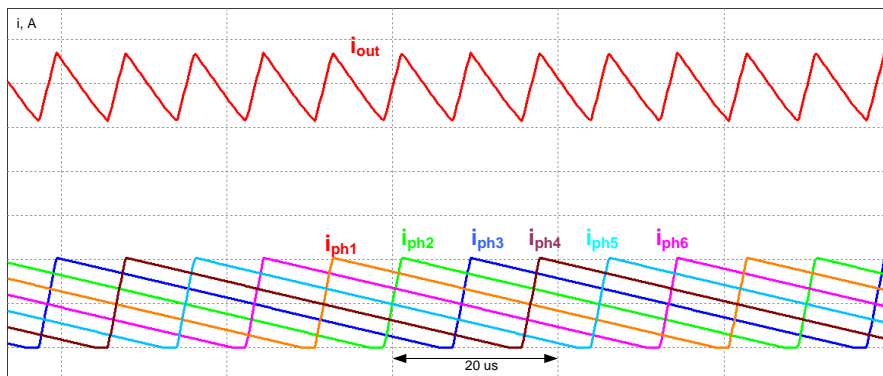


Fig. 5.7. The per-phase and output current of the converter.

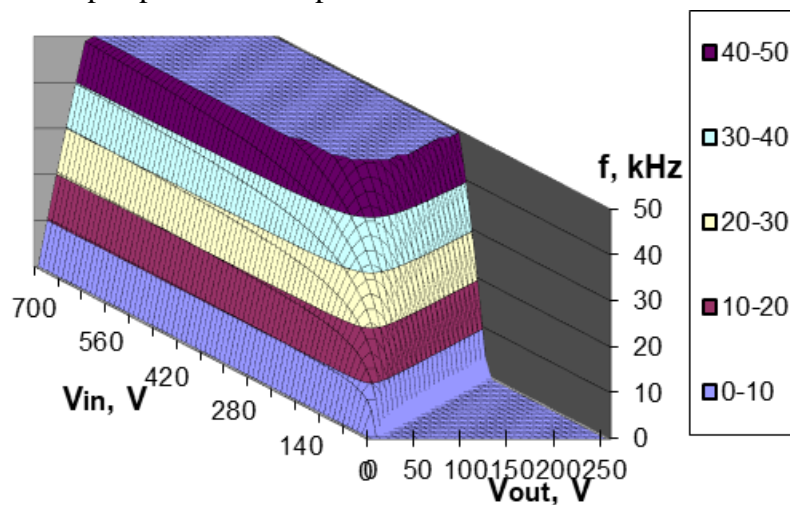


Fig. 5.8. Switching frequency of the DC-DC converter, $I_m = 5$ A.

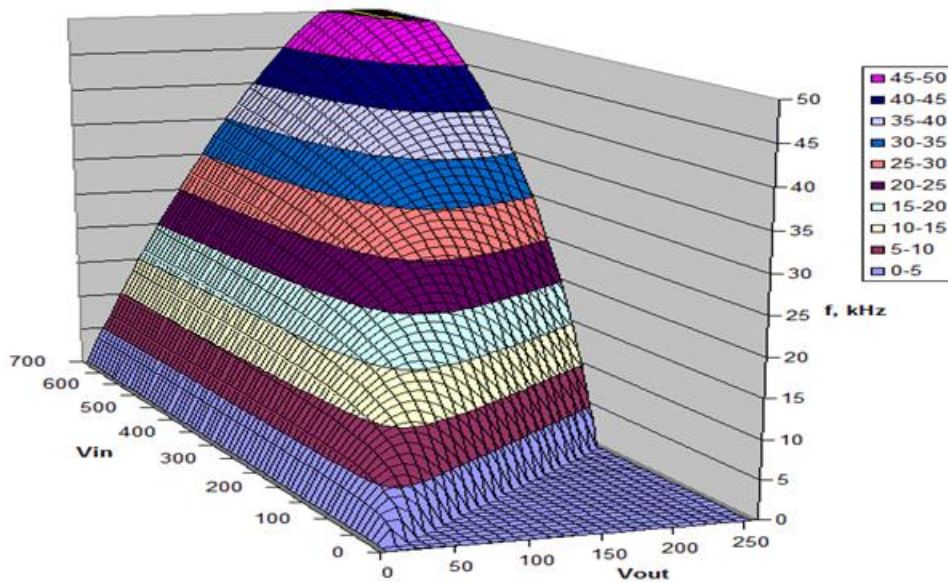


Fig. 5.9. Switching frequency of the DC-DC converter, $I_m = 20$ A.

According to (5.4) and (5.5) switching frequency is very high at a small value of I_m . This leads to high switching losses and too short time for calculation of the pulse length of the next period. Therefore, in such case it is beneficial to enlarge the value of I_m and decrease the switching frequency. This can be done by limiting the PWM period value in the software (Fig. 5.8 and 5.9). This results in the increasing of difference between the reference value and the actual value of the controlled parameter as well as I_m calculated by PI algorithm and the pulse length. This leads to the increasing of current while frequency stays equal to 50 kHz. This means that the converter works in deeper DCM mode.

5.1.3. Hardware

Fig. 5.10 shows the hardware implementation of the DSP controlled 6-phase interleaved bidirectional DC-DC converter. The power transistors (4) are placed on the radiator plate (5), MOSFET drivers (3) are located near to the transistors, and DSP board (2) is based on the STM32F407VGT6 microcontroller. In order to smoothen pulsations of current, the parallel connection of two 47 μ F electrolytic capacitors (6) is used. The converter is connected via contactors (1) to the DC bus and to the storage system after charging the filter capacitors through resistors.

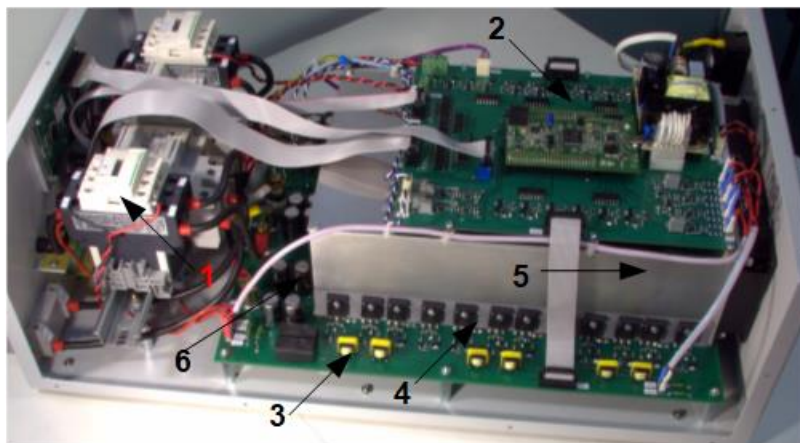


Fig. 5.10. Hardware of interleaved DC-DC converter.

If relevant control algorithm is implemented, the application of the converter can be extensive. In the particular case, algorithms for supercapacitor and for Li-ion battery are developed. In charging mode of the supercapacitor input voltage is regulated to accumulate all of the braking energy of the drive but in charging mode of the supercapacitor – output current. Li-ion battery is charged and discharged in current mode. Switching off of the transistors produces significant EMI. Therefore, it is important to measure current and voltage at the moment when switching of transistors does not take place. The transistors are controlled by DSP, and it is possible to calculate the switching times of the transistors and choose ADC conversion time without transistor switching. In order to improve the stability of the converter, the digital filtering of measured signals was used.

5.1.4. The test bench and experimental results

Fig. 5.11 shows the schematics of the AC induction motor drive test bench with two direct torque control (DTC) variable frequency drives (VFD) and induction motors. Due to the application of DTC frequency converters, the test bench could operate without torque sensor, which is required for most precise control only. Both AC machines M1 and M2 are mechanically coupled together; one of them imitates the elevator, and the second imitates the load. Motor M1 is operated in speed control mode while load simulator motor M2 operates in torque control mode. Nominal power and nominal speed of M1 and M2 is $P_{\text{nom,bench}} = 7.5 \text{ kW}$ and $n = 1440 \text{ rpm}$, respectively. Frequency converter of motor M2 includes a reversible rectifier. During the traction mode of the bench, whole electrical energy generated by M2 is transferred to AC grid, therefore, the test bench can be tested at full load as there is installed braking circuit connected to its DC link just for safety reasons.

The energy storage system (modernization device) that includes bi-directional DC-DC converter and series connection of supercapacitors is connected to the DC link of the traction drive simulator. The DC-DC converter operates in a buck mode at supercapacitor charging and boost mode at supercapacitor discharging. In the output of DC-DC converter two 125 V supercapacitor modules in series are connected with a maximum voltage equal to 250 V DC. Fig. 5.11 does not present the three-phase rectifier that is inside the VFD but DC bus is presented with 600 V DC network. In elevator drive, generator mode (braking mode) braking resistor Rbr1 circuit with its chopper will operate only if energy storage system is disconnected or fully charged. In this mode, the DC-DC converter regulates the DC bus voltage, and the reference voltage is below the limit of braking chopper. During this mode, the energy is stored into supercapacitors and utilized repeatedly during the next lifting cycle.

Figure 5.12 shows hardware of the developed test bench – in this case ABB VFDs, braking resistors, and CEO electric motors are used. The 2 supercapacitor modules Maxwell BDO-0063-P125-B01 with rated capacitance $C = 63 \text{ F}$ and nominal voltage $V_{\text{sc,nom}}=125 \text{ V}$ are applied. The test bench control system is developed to test on test the bench the bi-directional DC-DC converter for energy recovery application.

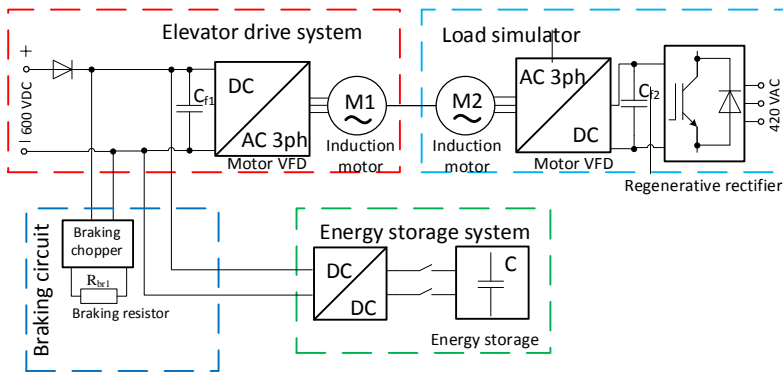


Fig. 5.11. Simplified diagram of the test bench.

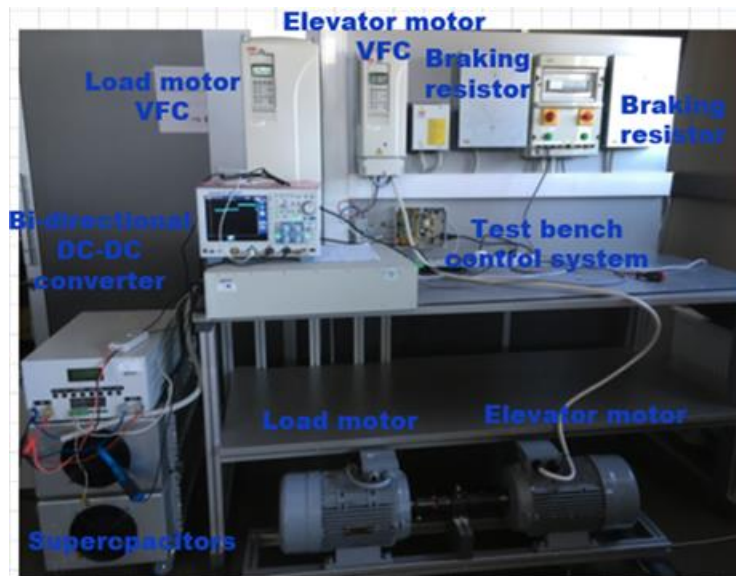


Fig. 5.12. Hardware implementation of the test bench.

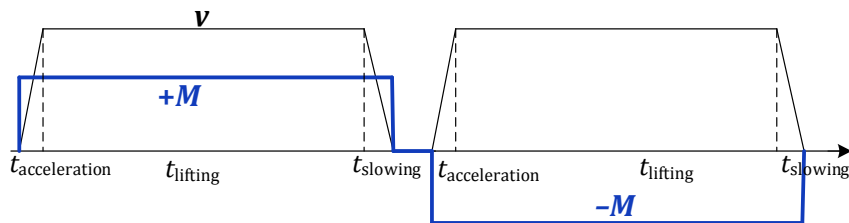


Fig. 5.13. The reference control signals sent to the analogs inputs of VFDs.

Fig. 5.13 shows control signals sent to VFDs. The elevator motor VFD is controlled by providing speed reference signal (black curve in Fig. 5.13). The elevator accelerates to the constant speed and then keeps constant speed until it slows down in the desired slowing down time. To the load emulation VFD is controlled by providing torque reference signal (blue curve in Fig. 5.13). During the braking mode, the control is designed to provide negative torque reference signal to load emulation VFD.

Figure 5.14 shows hardware implementation of the test bench control system. The relays are designed to send start and stop signals to VFDs, reverse direction signal to emulator motor VFD. STM32 microcontroller is used to generate control signal, AC-DC power supply with +15 V, -15 V and 5 V output voltages is used to supply power to DSP board, amplifiers and relays. Amplifier is

used to amplify 0–3.3 V signal to 0–10 V signal. To generate control signals, two digital-to-analog converter (DAC) signals are generated and then amplified.

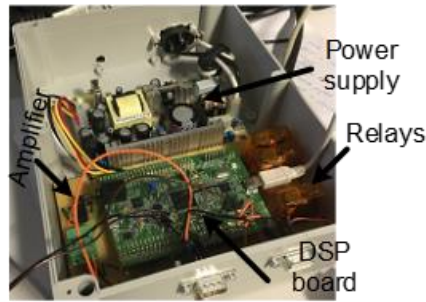


Fig. 5.14. Hardware implementation of the test bench control system.

Fig. 5.15 shows DC bus voltage of elevator motor VFD, it is possible to clearly indicate the braking time of period when the voltage goes up to the braking chopper operating voltage. If the storage is not installed, the energy is wasted in braking resistor as heat, therefore, long tests with high power are not possible as it will lead to overheating of the resistor. During the lifting mode, the voltage drops down.

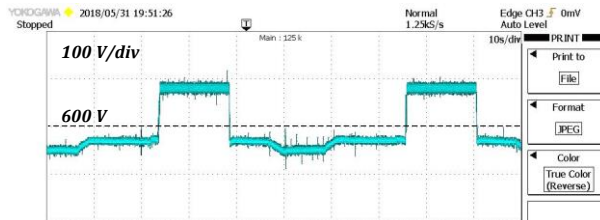


Fig. 5.15. Voltage of DC bus during two cycles implemented on test bench.

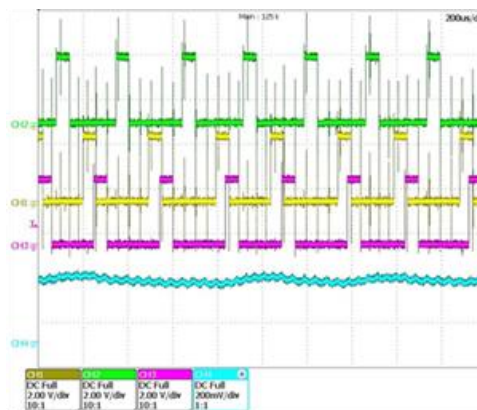


Fig. 5.16. Interleaved transistor control signals and current in discharge mode.

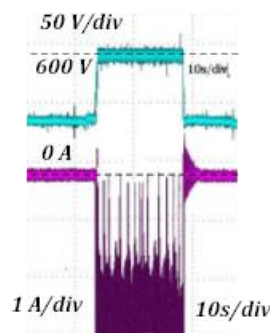


Fig. 5.17. DC bus voltage and current in charging mode.

Figure 5.16 shows current in discharging mode when energy is transferred to the drive system from the energy storage. It can be seen that the current has low ripple but the control system can be improved further to reduce lower frequency pulsations. The new duty cycle and period value as well as phase shift are calculated in each switching period, therefore, for higher switching frequencies the FPGA should be used to reduce calculation time. In this case, 168 MHz DSP was used and the calculations take 20 μ s so the highest switching frequency was limited to 50 kHz. As it can be seen in Fig. 5.16, the accurate phase shifting of interleaved signals can be implemented by updating timer value in regions where no switching actions take place.

Figure 5.17 shows experimental waveforms of DC bus voltage and converter input current in charging mode. In this mode as a reference signal 600 V DC bus voltage is used, and the converter controls this voltage to maintain it constant. The operation in this mode is stable, by increasing power the electromagnetic interference start plays the role that can influence proper operation of the converter, therefore, cable with shield should be used.

As the prototype was developed to test experimentally proposed control algorithm and topology, further increase of efficiency is possible by implementing synchronous rectification, soft turn off of the transistors, also optimization of magnetic components is possible. Current tests show efficiency close to 95 %, it means that very high efficiency can be achieved by using such an approach. The control algorithm is tested and the switching frequency can be increased by using FPGA or faster microcontrollers. The main problem that should be eliminated is voltage misbalance process that takes place, therefore, in further designs balancing circuit or special control method should be implemented.

5.2. ISOP forward converter and proposed voltage balancing method for low voltage supercapacitor module integration

As the voltage of one supercapacitor cell is equal to approximately 3 V, in the case of low power energy storage is required, the voltage of supercapacitors or Li-ion battery will be low – it means that an isolated DC-DC converter is required to provide energy flow between 1 phase or 3 phase DC bus and energy storage. In this case, unidirectional DC-DC converter, that allows to store regenerative braking energy and then use this energy to supply electricity to DC loads, for example, LED lightening, is proposed.

5.2.1. Converter description

As proper converter topology for such application input-series output-parallel (ISOP) configuration is selected that consists of two modular DC-DC converters connected in series at the input and in parallel at the output (Fig. 5.18), enabling the use of high switching frequency MOSFETs with low voltage ratings, which leads to a higher power density and a high conversion efficiency. As output current ripple frequency is twice of the switching frequency, size and costs of the output filter can be reduced. The voltage of both legs of the converter due to unequal values of passive components and delays in control signals may differ. If this issue is solved without changing the control system, the control of the converter can be realized as for conventional DC-DC converter just signals should be shifted in phase by 180°.

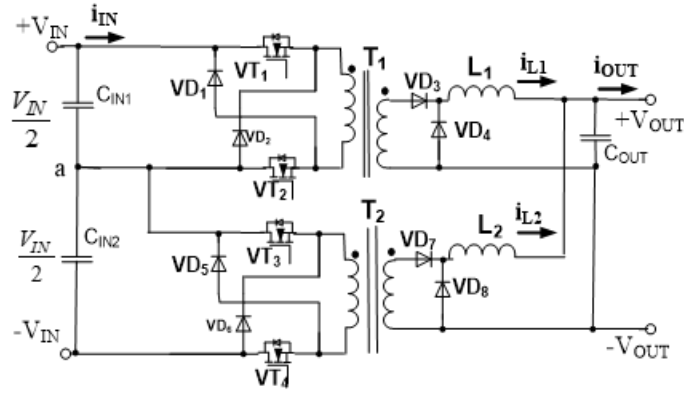


Fig. 5.18. Schematics of ISOP forward DC-DC converter.

If in the ISOP the converter balancing of the voltages of both legs is not provided, the difference in currents through transistors causes misbalance of the capacitors voltage and this will lead to failure. The difference of currents of both legs can be caused by unequal inductances of the inductors, transformers, unlike parameters of semiconductors or different duty cycle, especially, in the transient process. Misbalance in the voltage causes larger current in the leg with higher voltage so slow process of stabilization will take place, but mostly it is not enough to keep voltage of the capacitor in the desired level. Therefore, it is necessary to find a solution to prevent the situation when voltage of the capacitor reaches dangerous value and damages semiconductors or passive elements. Further the balancing circuit that is simple with as small as possible power losses and allows significantly easier implement closed loop control of the converter – even by using traditional integrated circuits, will be analyzed.

5.2.2. The proposed balancing method

In [64], combination of two transformers by integrating them in one magnetic core are used to balance the input voltages, in [65], equal duty cycle is utilized to balance the input voltages: the module with higher input voltage supplies more current. For interleaved converter common duty cycle in the transient process cannot be realized. In papers [66], [67], input voltage feedback loops are applied to balance the input voltage. This complicates the design of the control system, isolated high voltage sensing circuit is required, and therefore voltage balancing method that allows equal input voltage sharing in a simple way without complex control system is proposed.

The proposed voltage balancing circuit for the input-series-output parallel connected converter configuration is shown in Fig. 5.19 for medium-voltage power conversion applications, but such circuit can be used in other isolated configurations, too. The input-series output-parallel (ISOP) configuration consists of two modular DC-DC converters connected in series at the input and in parallel at the output, enabling the use of MOSFET transistors with low voltage ratings, which leads to a high power density and a high conversion efficiency. As output current ripple frequency is twice the switching frequency, size and costs of the output filter can be reduced. The control of the converter is realized by using analogue circuit realized in an analog chip.

Figure 5.19 shows basic schematics of the converter and balancing circuit. The balancing circuit consists of additional winding of transformer with number of windings equal to the number of the windings of the primary side of the pulse transformer. In the series with this winding the resistor R_1 is connected, which limits the balancing current and diode VD_3 to prevent power losses in the

resistor if voltage of capacitor is higher than voltage of balancing winding. Figure 5.19 explains the operational principle of the proposed circuit. If the voltages on input capacitors differ, during the on time of the corresponding transistor balancing current flows from balancing winding to the capacitor and partly compensates current i_N thus gradually equalizing the voltage levels of both capacitors. The voltage levels cannot be equalized to equal values, but it is not necessary in this case, as the main task of the balancing is to prevent dangerous values of the voltage, moreover, additional circuit is implemented that switches off the converter if the voltage of one of the capacitors becomes critically high. The power losses in the resistor can be expressed as follows:

$$P_{\text{balancing}} < 2\Delta U i_N. \quad (5.7)$$

The power losses in this circuit are low therefore compact balancing resistor can be used with power of several watts, additional balancing windings can be created by using wire with small cross-sectional area. The experimental results demonstrate that the voltage of both capacitors in all operating modes stays equal and the measured temperature of the balancing resistors is less than 50°C . This means that the balancing losses are small and the proposed method is suitable for practical application.

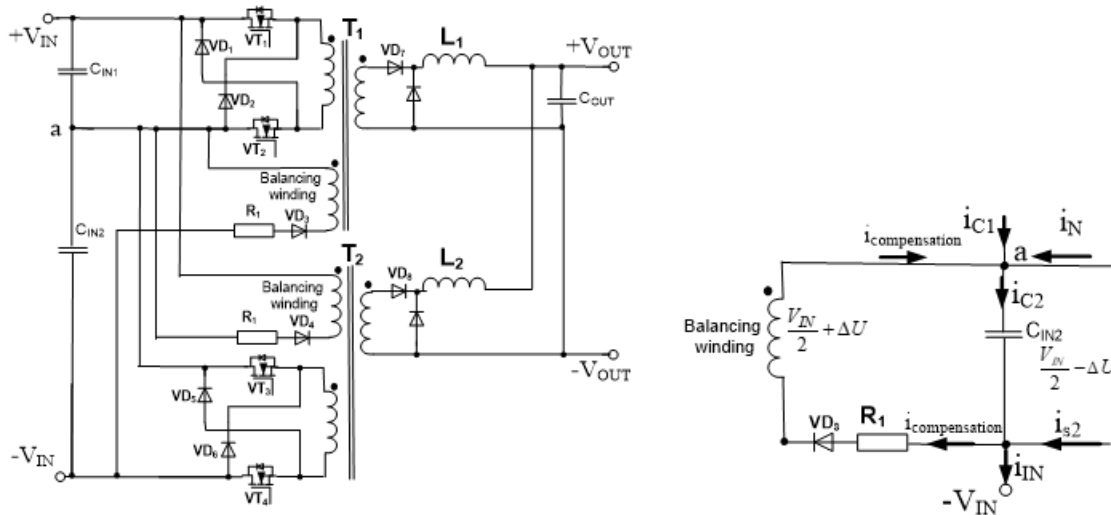


Fig. 5.19. Input-series-output parallel DC-DC converter with balancing circuit [68].

Figure 5.20 shows the structure of the proposed transformer with integrated balancing winding, which consists of round ferrite core and three windings. Number of turns of the secondary winding and balancing winding are equal to 27. For the balancing winding a wire with cross sectional area equal to 0.2 mm^2 is used. For the secondary winding a litz wire with cross sectional area equal to 7 mm^2 is used.

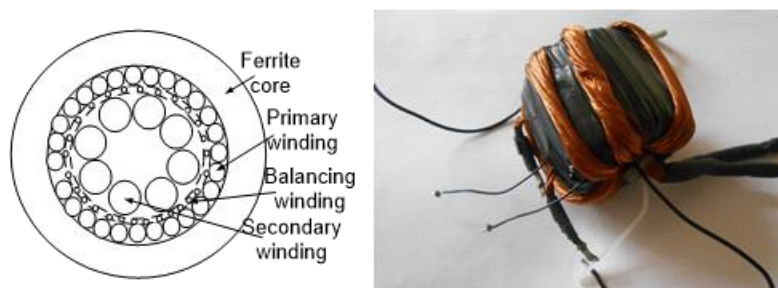


Fig. 5.20. Transformer with integrated balancing winding.

5.2.3. The prototype and test results

The particular converter is designed for input voltage 600 V DC and output voltage from 0 V to 30 V, output current 100 A. The control of the converter is realized in two approaches: by using DSP microcontroller or analog control circuit [68]. Figure 5.21 shows hardware of the converter.

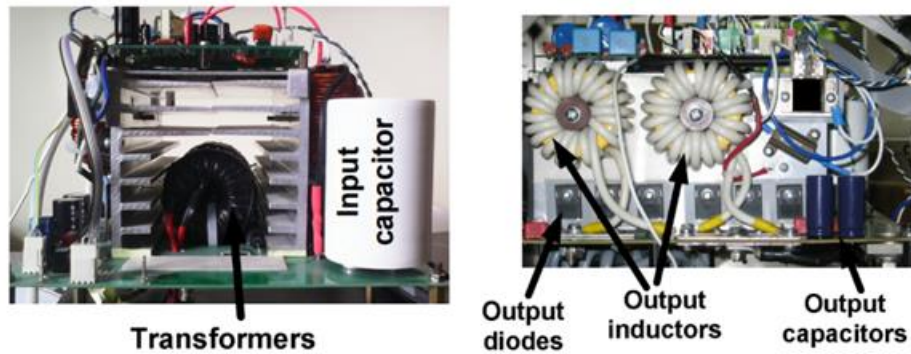


Fig. 5.21. Hardware realization of the ISOP DC-DC converter.

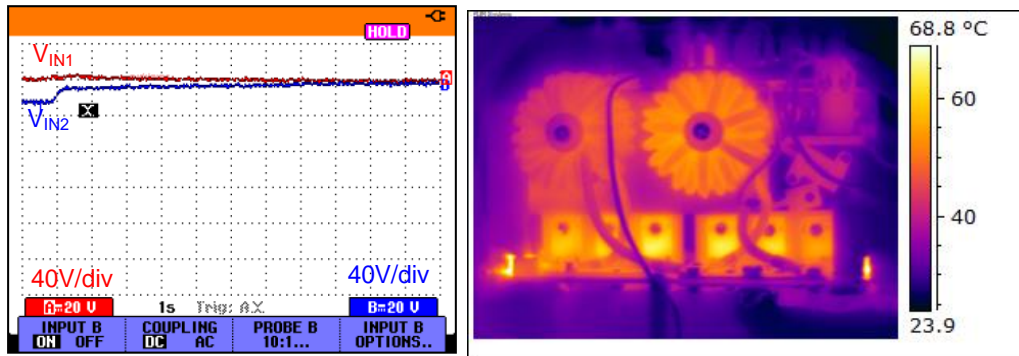


Fig. 5.22. Voltage balancing process and thermal image of the converter.

Figure 5.22 shows the thermal image of the converter with the hottest spots. To cool down the semiconductors and magnetic elements, the converter is equipped with a radiator and electric air exhauster. In the oscillogram, shown in Fig. 5.22, in the beginning the converter works with full load, therefore, voltage balancing circuit cannot fully compensate misbalance current, but the voltage stays in the safety margin. After the reducing of the load, balancing circuit equalizes both voltages. The oscillogram is measured in the short circuit and no load conditions in which the voltage equalizing process is the worst as duty cycle in these modes are small. However, even in the following conditions balancing circuit works satisfactorily.

The voltage balancing of the capacitors of the multilevel converter can be a big challenge. The proposed method enables solving this problem without implementation of additional control loop. The circuit is simple and cheap, it enables preventing the rising of the capacitor voltage to the dangerous voltage with negligible power losses. The proposed circuit is useful also for other types of isolated multilevel converters.

Conclusions

The regulated electric drive is used extensively, and it is expected that the electric drive application will continue to grow. Even a small increase in energy efficiency can bring great impact on total energy savings. In many applications regenerative braking energy is still wasted as a heat, by implementing supercapacitor based modernization device, the energy efficiency of the drive can be significantly improved. For example, in the case of a crane used to transport containers in a port, it can be concluded that the efficiency of electric cranes can be increased by as much as 40 %, which makes it possible to calculate payback time of such a device equal to 5 years.

The developed regenerative braking energy test bench allows studying the energy processes in the traction drive, however, exact research also requires the coincidence of the research machine used on the bench. On the stand, it is possible to study the power electronics and their control methods, as well as various algorithms for energy storage control. The developed test bench was used to test the supercapacitor based modernization kit. With such a conversion kit, it is possible to equip a light electric vehicle by improving the efficiency and peak power by extending lifetime of lead-acid battery.

The work studies the possibilities of using magnetically coupled inductors in different configurations. As a result, analytical formulas have been obtained, which can be used for calculation of current pulsations in practical applications. The obtained relationships allow concluding that the use of such inductors reduces current pulsations and thus increases the efficiency of the converter. The work uses a relatively simple construction of magnetically coupled inductors, which allows more easily to implement such solutions in practical applications. The coupled inductors are implemented in several prototypes, experimental results confirm theoretical results.

The use of a supercapacitor based modernization device for starting internal combustion engines is a promising solution. As supercapacitors are relatively expensive at this time, it is proposed to use supercapacitors with less capacity by using active semiconductor based switches. This allows to eliminate voltage drop in the short-circuit mode at the start-up phase, prolong lead-acid battery life and act as a backup power source for the battery in case of discharge.

The proposed non-isolated bi-directional DC-DC converter topology allows to reduce the size of the converter because of the use of boundary conduction mode. The developed control method allows control of the converter without current control in individual converter phases. The algorithm for selection of time intervals without switching transitions for analogue value measurement allows to reduce the influence of electromagnetic interference on the measurement results. The use of a digital filter ensures more precise calculation of the period and pulse widths. The proposed current ripple reduction method by changing the number of active phases allows further reduction of current ripples.

The proposed voltage balancing method for multilevel isolated DC-DC converters allows to realize voltage balancing without introducing an additional voltage control loop and without input voltage measurement. The use of a multilevel structure enables the use of MOSFET transistors with better parameters, potentially allowing to improve converter efficiency.

If the price of supercapacitors decreases, they will become widely used in many areas as they have high power density and high number of charge/discharge cycles. In most applications, tailor-made for a particular application power electronics will be required to provide optimal power flow control. This work presents new solutions for the use of supercapacitors for modernization of existing electric drive systems, in these solutions power electronics converter is one of the main components. The proposed solutions can be further developed both as scientific research and as commercial products.

In each application, the power electronics converter has different requirements – the most important in transport is the size, in the case of industrial drives – reliability and price. In this Doctoral Thesis research has been carried out to reduce the size of the converter for transport use, and in order to reduce the converter price and shorten the response time for industrial application. Initial research in the field of DC-DC converters should be continued in an effort to achieve even better results, and it is also important to further explore the methods for managing optimal energy flow in the to and from energy storage. The developed converter proposed for the energy storage integration in a drive system for regenerative braking energy should be improved further to eliminate the voltage imbalance problem and reduce switching losses, as well as the use of SiC and GaN transistors to maximize efficiency can be considered. This work will promote wider use of supercapacitor energy storages in new applications, as well as contribute to future research on DC-DC converters for energy storage systems.

Literature

- [1] “Microsoft Word - Climate-Foundation-IIP-Motor-Systems Report -5-Sept-2011.docx - IIPmotorsystems_report11.pdf.” [Online]. Available: http://www.iipnetwork.org/sites/iipnetwork.org/themes/iipnetwork/downloads/IIPmotorsystems_report11.pdf. [Accessed: 04-Feb-2016].
- [2] N. Jabbour and C. Mademlis, “Supercapacitor-Based Energy Recovery System With Improved Power Control and Energy Management for Elevator Applications,” *IEEE Trans. Power Electron.*, vol. 32, no. 12, pp. 9389–9399, Dec. 2017.
- [3] “European Commission. Final energy consumption per sector.” [Online]. Available: <http://ec.europa.eu/eurostat/tgm/graph.do?tab=graph&plugin=1&pcode=tsdpc320&language=en&toolbox=data>. [Accessed: 26-Mar-2017].
- [4] “Market outlook to 2022 for battery electric vehicles and plug-in hybrid electric vehicles.” [Online]. Available: <https://www.theccc.org.uk/archive/aws2/docs/CH6%20-%20AEA%20-%20Market%20outlook%20to%202022%20for%20battery%20electric%20vehicles%20and%20plug-in%20hybrid%20electric%20vehicles.pdf>. [Accessed: 26-Mar-2017].
- [5] A. von Jouanne, P. N. Enjeti, and B. Banerjee, “Assessment of ride-through alternatives for adjustable-speed drives,” *IEEE Trans. Ind. Appl.*, vol. 35, no. 4, pp. 908–916, July 1999.
- [6] S. Yang, A. Bryant, P. Mawby, D. Xiang, L. Ran, and P. Tavner, “An Industry-Based Survey of Reliability in Power Electronic Converters,” *IEEE Trans. Ind. Appl.*, vol. 47, no. 3, pp. 1441–1451, May 2011.
- [7] A. D. Napoli and A. Ndokaj, “Ultracapacitor storage for a 50t capacity gantry crane,” in *2012 XXth International Conference on Electrical Machines*, 2012, pp. 2014–2018.
- [8] A. Ndokaj, A. D. Napoli, G. Pede, and M. Pasquali, “Regulation strategy of an Ultracapacitor storage model for a gantry crane,” in *IECON 2013 - 39th Annual Conference of the IEEE Industrial Electronics Society*, 2013, pp. 1209–1216.
- [9] T. S. Kwon et al., “Power Control Algorithm for Hybrid Excavator with Super Capacitor,” in *2008 IEEE Industry Applications Society Annual Meeting*, 2008, pp. 1–8.
- [10] N. Zhao, N. Schofield, and W. Niu, “Energy Storage System for a Port Crane Hybrid Power-Train,” *IEEE Trans. Transp. Electrification*, vol. 2, no. 4, pp. 480–492, Dec. 2016.
- [11] A. Luque et al., “Energy reduction on eRTG,” in *2016 IEEE 16th International Conference on Environment and Electrical Engineering (EEEIC)*, 2016, pp. 1–6.
- [12] S. M. Kim and S. K. Sul, “Control of Rubber Tyred Gantry Crane With Energy Storage Based on Supercapacitor Bank,” *IEEE Trans. Power Electron.*, vol. 21, no. 5, pp. 1420–1427, Sep. 2006.
- [13] P. Fajri, R. Ahmadi, and M. Ferdowsi, “Equivalent vehicle rotational inertia used for electric vehicle test bench dynamic studies,” in *IECON 2012 – 38th Annual Conference on IEEE Industrial Electronics Society*, 2012, pp. 4115–4120.
- [14] H. Takagi, “Real-Life Coefficient of Drag — a Simple Extraction Method,” *AutoTechnology*, vol. 5, no. 4, pp. 52–56, Jul. 2005.
- [15] V. Brazis, K. Kroics, and L. Grigans, “Scientific Laboratory Platform for Testing the Electric Vehicle Equipped with DC Drive,” *Latv. J. Phys. Tech. Sci.*, vol. 51, no. 5, pp. 56–64, 2014.

- [16] K. Kroichs and V. Brazis, "A Digitally Controlled Test Bench for DC Electrical Drives," in Proceedings in Multidisciplinary Conference QUAESTI, Slovakia, Zilina, 2013, pp. 166–170.
- [17] K. Kroichs, V. Brazis, and others, "Digitally controlled synchronous buck-boost converter for ultracapacitor based energy storage application," Eng. Rural Dev. Latv., 2014.
- [18] J. Larminie and J. Lowry, "Front Matter," in Electric Vehicle Technology Explained, John Wiley & Sons, Ltd, 2012, pp. i–xxv.
- [19] G. Randolph, Final report of the battery life extension experiment. University of Hawaii and Hawaii Electric Vehicle Demonstration Project, Spring, 1999.
- [20] G. Papazov and D. Pavlov, "Influence of cycling current and power profiles on the cycle life of lead/acid batteries," J. Power Sources, vol. 62, no. 2, pp. 193–199, 1996.
- [21] A. W. Stienecker, T. Stuart, and C. Ashtiani, "A combined ultracapacitor-lead acid battery storage system for mild hybrid electric vehicles," in 2005 IEEE Vehicle Power and Propulsion Conference, 2005.
- [22] B. Hredzak, V. G. Agelidis, and G. D. Demetriades, "A Low Complexity Control System for a Hybrid DC Power Source Based on Ultracapacitor #x2013;Lead #x2013;Acid Battery Configuration," IEEE Trans. Power Electron., vol. 29, no. 6, pp. 2882–2891, Jun. 2014.
- [23] K. Kroichs and V. Brazis, "Ultracapacitor based storage system for lead-acid powered light electric vehicle retrofit," presented at the Engineering for Rural Development, 2016, vol. January 2016, pp. 1386–1394.
- [24] "Electric Golf Cart Oc Gc | Free Images at Clker.com - vector clip art online, royalty free & public domain." [Online]. Available: <http://www.clker.com/clipart-70567.html>. [Accessed: 18-Aug-2016].
- [25] K. Kroichs and V. Brazis, "Supercapacitor based storage system for efficiency improvement of lead-acid powered light electric vehicle," in 2016 IEEE International Power Electronics and Motion Control Conference (PEMC), 2016, pp. 1216–1221.
- [26] Pit-Leong Wong, Q. Wu, Peng Xu, Bo Yang, and F. C. Lee, "Investigating coupling inductors in the interleaving QSW VRM," 2000, vol. 2, pp. 973–978.
- [27] B. Oraw and R. Ayyanar, "Stability of multi-winding coupled inductors in buck converters," in INTEC 2008 - 2008 IEEE 30th International Telecommunications Energy Conference, 2008, pp. 1–6.
- [28] R. S. Balog and P. T. Krein, "Coupled-Inductor Filter: A Basic Filter Building Block," IEEE Trans. Power Electron., vol. 28, no. 1, pp. 537–546, Jan. 2013.
- [29] M. L. Bolloch, M. Cousineau, and T. Meynard, "Current-sharing control technique for interleaving VRMs using intercell transformers," in 13th European Conference on Power Electronics and Applications, 2009. EPE'09, 2009, pp. 1–10.
- [30] E. Duran, J. M. Enrique, M. A. Bohorquez, M. Sidrach-de-Cardona, J. E. Carretero, and J. M. Andujar, "A new application of the coupled-inductors SEPIC converter to obtain I-V and P-V curves of photovoltaic modules," in 2005 European Conference on Power Electronics and Applications, 2005.
- [31] D. C. Hamill and P. T. Krein, "A 'zero' ripple technique applicable to any DC converter," in 30th Annual IEEE Power Electronics Specialists Conference, 1999. PESC 99, 1999, vol. 2, pp. 1165–1171.

- [32] J. W. Kolar, H. Sree, N. Mohan, and F. C. Zach, "Novel aspects of an application of 'zero'-ripple techniques to basic converter topologies," in , 28th Annual IEEE Power Electronics Specialists Conference, 1997. PESC'97 Record, 1997, vol. 1, pp. 796–803.
- [33] J. W. Kolar, H. Sree, N. Mohan, and F. C. Zach, "Novel aspects of an application of 'zero'-ripple techniques to basic converter topologies," in , 28th Annual IEEE Power Electronics Specialists Conference, 1997. PESC'97 Record, 1997, vol. 1, pp. 796–803.
- [34] D. Maksimovic, R. W. Erickson, and C. Griesbach, "Modeling of cross-regulation in converters containing coupled inductors," *IEEE Trans. Power Electron.*, vol. 15, no. 4, pp. 607–615, July 2000.
- [35] H. N. Nagaraja, D. Kastha, and A. Petra, "Design Principles of a Symmetrically Coupled Inductor Structure for Multiphase Synchronous Buck Converters," *IEEE Trans. Ind. Electron.*, vol. 58, no. 3, pp. 988–997, Mar. 2011.
- [36] K. Kroics, U. Sirmelis, and V. Brazis, "Design of coupled inductor for interleaved boost converter," *Przeglad Elektrotechniczny*, vol. 2014, no. 12, pp. 91–94.
- [37] K. Kroics, U. Sirmelis, L. Grigans, and V. Brazis, "Digitally controlled 4-phase interleaved DC-DC converter with coupled inductors for storage application in microgrid," presented at the Proceedings - 2015 9th International Conference on Compatibility and Power Electronics, CPE 2015, 2015, pp. 504–509.
- [38] W. Chen, X. Huang, and J. Zheng, "Improved winding loss theoretical calculation of magnetic component with air-gap," in *Power Electronics and Motion Control Conference (IPEMC)*, 2012 7th International, 2012, vol. 1, pp. 471–475.
- [39] K. Kroics, J. Zakis, and U. Sirmelis, "Multiphase interleaved DC-DC converter with directly and inversely coupled inductors," in *2016 57th International Scientific Conference on Power and Electrical Engineering of Riga Technical University (RTUCON)*, 2016, pp. 1–6.
- [40] A. W. Stienecker, T. Stuart, and C. Ashtiani, "A combined ultracapacitor-lead acid battery storage system for mild hybrid electric vehicles," in *2005 IEEE Vehicle Power and Propulsion Conference*, 2005.
- [41] W. Henson, "Optimal battery/ultracapacitor storage combination," *J. Power Sources*, vol. 179, no. 1, pp. 417–423, Apr. 2008.
- [42] R. A. Dougal, S. Liu, and R. E. White, "Power and life extension of battery-ultracapacitor hybrids," *IEEE Trans. Compon. Packag. Technol.*, vol. 25, no. 1, pp. 120–131, Mar. 2002.
- [43] J. P. Zheng, T. R. Jow, and M. S. Ding, "Hybrid power sources for pulsed current applications," *IEEE Trans. Aerosp. Electron. Syst.*, vol. 37, no. 1, pp. 288–292, Jan. 2001.
- [44] L. Solero, A. Lidozzi, and J. A. Pomilio, "Design of multiple-input power converter for hybrid vehicles," *IEEE Trans. Power Electron.*, vol. 20, no. 5, pp. 1007–1016, Sep. 2005.
- [45] A. F. Burke, "Batteries and Ultracapacitors for Electric, Hybrid, and Fuel Cell Vehicles," *Proc. IEEE*, vol. 95, no. 4, pp. 806–820, Apr. 2007.
- [46] J. M. Blanes, R. Gutiérrez, A. Garrigós, J. L. Lizán, and J. M. Cuadrado, "Electric Vehicle Battery Life Extension Using Ultracapacitors and an FPGA Controlled Interleaved Buck-Boost Converter," *IEEE Trans. Power Electron.*, vol. 28, no. 12, pp. 5940–5948, Dec. 2013.
- [47] K. Kroics, "System for start of internal combustion engine with hybrid battery-supercapacitor source," in *2015 56th International Scientific Conference on Power and Electrical Engineering of Riga Technical University (RTUCON)*, 2015, pp. 1–6.

- [48] J. B. Olson and E. D. Sexton, "Operation of lead-acid batteries for HEV applications," in *Battery Conference on Applications and Advances*, 2000. The Fifteenth Annual, 2000, pp. 205–210.
- [49] S. Breban, M. Nasser, A. Vergnol, B. Robyns, and M. M. Radulescu, "Hybrid wind/microhydro power system associated with a supercapacitor energy storage device - experimental results," in *18th International Conference on Electrical Machines*, 2008. ICEM 2008, 2008, pp. 1–6.
- [50] "Converter for energy storage integration in photovoltaic plants," in *Proceedings of the 2002 IEEE International Symposium on Industrial Electronics*, 2002. ISIE 2002, 2002, vol. 3, pp. 959–963.
- [51] P.-L. Wong, P. Xu, P. Yang, and F. C. Lee, "Performance improvements of interleaving VRMs with coupling inductors," *IEEE Trans. Power Electron.*, vol. 16, no. 4, pp. 499–507, Jul. 2001.
- [52] Y. Panov and M. M. Jovanovic, "Design considerations for 12-V/1.5-V, 50-A voltage regulator modules," *IEEE Trans. Power Electron.*, vol. 16, no. 6, pp. 776–783, Nov. 2001.
- [53] J. Shen, K. Righers, and R. W. D. Doncker, "A Novel Phase-Interleaving Algorithm for Multiterminal Systems," *IEEE Trans. Power Electron.*, vol. 25, no. 3, pp. 741–750, Mar. 2010.
- [54] M. Hirakawa et al., "High power DC/DC converter using extreme close-coupled inductors aimed for electric vehicles," in *Power Electronics Conference (IPEC), 2010 International*, 2010, pp. 2941–2948.
- [55] J. Shen, K. Righers, and R. W. D. Doncker, "A Novel Phase-Interleaving Algorithm for Multiterminal Systems," *IEEE Trans. Power Electron.*, vol. 25, no. 3, pp. 741–750, Mar. 2010.
- [56] O. Garcia, P. Zumel, A. de Castro, J. A. Cobos, and J. Uceda, "An automotive 16 phases DC-DC converter," in *Power Electronics Specialists Conference, 2004. PESC 04. 2004 IEEE 35th Annual*, 2004, vol. 1, pp. 350-355.
- [57] P. Nandankar and M. V. Aware, "High efficiency discontinuous mode interleaved multiphase bidirectional dc-dc converter," in *2012 IEEE International Conference on Power Electronics, Drives and Energy Systems (PEDES)*, 2012, pp. 1–6.
- [58] L. Huber, B. T. Irving, and M. M. Jovanovic, "Open-Loop Control Methods for Interleaved DCM/CCM Boundary Boost PFC Converters," *IEEE Trans. Power Electron.*, vol. 23, no. 4, pp. 1649–1657, Jul. 2008.
- [59] J. R. Tsai, T. F. Wu, C. Y. Wu, Y. M. Chen, and M. C. Lee, "Interleaving Phase Shifters for Critical-Mode Boost PFC," *IEEE Trans. Power Electron.*, vol. 23, no. 3, pp. 1348–1357, May 2008.
- [60] K. Kroics, "Bi-directional two level 6-phase DC-DC converter for energy storage application," in *Proceedings of PCIM Europe 2015; International Exhibition and Conference for Power Electronics, Intelligent Motion, Renewable Energy and Energy Management*, 2015, pp. 1–8.
- [61] P. J. Grbovic, P. Delarue, P. L. Moigne, and P. Bartholomeus, "The Ultracapacitor-Based Controlled Electric Drives With Braking and Ride-Through Capability: Overview and Analysis," *IEEE Trans. Ind. Electron.*, vol. 58, no. 3, pp. 925–936, Mar. 2011.

- [62] D. Gerber and J. Biela, "Interleaving of a Soft-Switching Boost Converter Operated in Boundary Conduction Mode," *IEEE Trans. Plasma Sci.*, vol. 43, no. 10, pp. 3374–3380, Oct. 2015.
- [63] Christopher Oliver, "A new core loss model for iron powder material." [Online]. Available: <http://www.micrometalsarnoldpowdercores.com/upload/Core%20Loss%20Update.pdf>. [Accessed: 08-May-2016].
- [64] S. Yang, Y. Fang, X. Qiu, and C. Gong, "Voltage Sharing Control for Interleaving Series-Parallel Dual Two-Transistor Forward Converter," in *33rd Annual Conference of the IEEE Industrial Electronics Society, 2007. IECON 2007, 2007*, pp. 1896–1900.
- [65] R. Giri, V. Choudhary, R. Ayyanar, and N. Mohan, "Common-duty-ratio control of input-series connected modular DC-DC converters with active input voltage and load-current sharing," *IEEE Trans. Ind. Appl.*, vol. 42, no. 4, pp. 1101–1111, Jul. 2006.
- [66] R. Giri, R. Ayyanar, and E. Ledezma, "Input-series and output-series connected modular DC-DC converters with active input voltage and output voltage sharing," in *Nineteenth Annual IEEE Applied Power Electronics Conference and Exposition, 2004. APEC'04, 2004*, vol. 3, pp. 1751-1756.
- [67] A. Bhinge, N. Mohan, R. Giri, and R. Ayyanar, "Series-parallel connection of DC-DC converter modules with active sharing of input voltage and load current," in *Seventeenth Annual IEEE Applied Power Electronics Conference and Exposition, 2002. APEC 2002, 2002*, vol. 2, pp. 648–653.
- [68] K. Kroics, J. Zakis, A. Suzdalenko, and G. Gaigals, "A simplified approach to input voltage balancing for series connected isolated DC-DC converters," in *2016 18th European Conference on Power Electronics and Applications (EPE'16 ECCE Europe), 2016*, pp. 1–10.